This is an open access article published under an ACS AuthorChoice License, which permits copying and redistribution of the article or any adaptations for non-commercial purposes.

JACS
JOURNAL OF THE AMERICAN CHEMICAL SOCIETY

Article

pubs.acs.org/JACS

Diversity of Secondary Structure in Catalytic Peptides with β-Turn-Biased Sequences

Anthony J. Metrano, Nadia C. Abascal, Brandon Q. Mercado, Eric K. Paulson, Anna E. Hurtley, and Scott J. Miller*

Department of Chemistry, Yale University, P.O. Box 208107, New Haven, Connecticut 06520-8107, United States

Supporting Information

ABSTRACT: X-ray crystallography has been applied to the structural analysis of a series of tetrapeptides that were previously assessed for catalytic activity in an atroposelective bromination reaction. Common to the series is a central Pro-Xaa sequence, where Pro is either L- or D-proline, which was chosen to favor nucleation of canonical β-turn secondary structures. Crystallographic analysis of 35 different peptide sequences revealed a range of conformational states. The observed differences appear not only in cases where the Pro-Xaa loop-region is altered, but also when seemingly subtle alterations to the flanking residues are introduced. In many instances, distinct conformers of the same sequence were observed, either as symmetry-independent molecules within the same unit cell or as polymorphs. Computational studies using DFT provided additional insight into the analysis of solid-state structural features. Select X-ray crystal structures were compared to the corresponding solution structures derived from measured proton chemical shifts, ^{3}J-values, and $^{1}H-^{1}H$-NOESY contacts. These findings imply that the conformational space available to simple peptide-based catalysts is more diverse than precedent might suggest. The direct observation of multiple ground state conformations for peptides of this family, as well as the dynamic processes associated with conformational equilibria, underscore not only the challenge of designing peptide-based catalysts, but also the difficulty in predicting their accessible transition states. These findings implicate the advantages of low-barrier interconversions between conformations of peptide-based catalysts for multistep, enantioselective reactions.

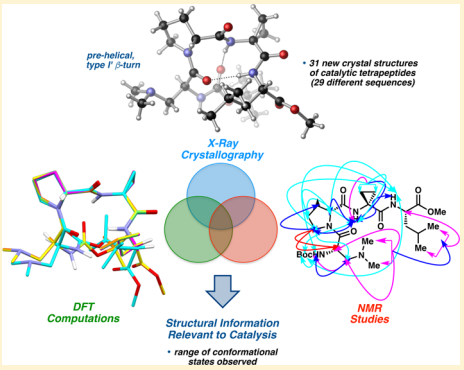

INTRODUCTION

Nature has evolved the capacity to catalyze chemical reactions with remarkable rate acceleration and selectivity. The catalytic efficacy of enzymes stems, in part, from their well defined, folded structures. Within the active site, catalytic residues are precisely oriented in space to accommodate well orchestrated, and often highly stabilized, transition states. Thus, a significant kinetic advantage is provided by active site preorganization, which itself is enforced and buttressed by the folded structure of the protein.[1] An ongoing goal of structural biology has been to develop a means to predict the folding patterns of proteins based solely on their primary amino acid sequences.[2] Endeavors to this end have produced important advances in the field, including analyses of structural trends from the protein data bank.[3] These studies have not only increased our collective understanding of protein secondary structures, but they have also provided a platform for the design of other peptidic systems, such as synthetic foldamers[4] and molecular devices.[5]

One interdisciplinary approach in the field of asymmetric catalysis for organic synthesis involves the design of minimal peptides that aim to capture key features of enzymatic active sites within a substantially simplified chiral environment. We,[6] and others,[7] have pursued this goal in recent years, which has led to the development of a variety of peptide-based catalysts that mediate asymmetric reactions. In general, catalysts of this type have been identified by implementation of either high-throughput screening[8] or hypothesis-driven design.[9] Whereas on-bead screening has delivered highly effective catalyst sequences that may not have been predicted on the basis of structural attributes, efforts to design peptide-based catalysts rationally have largely focused on sequences that are predisposed to certain secondary structures. The β-turn motif[10] has proven particularly fruitful in this regard. Inspired by comprehensive analyses of trends from the protein data bank,[3,10] as well as pioneering studies of low-molecular-weight peptides in organic solution,[11] we sought to take advantage of predictable β-turn geometry in our catalyst design. In many cases, the tendency of certain β-turn-containing peptides to adopt hairpin structures provides further conformational support through an additional interstrand hydrogen bond (H-bond).[12] This approach allows for the possibility of positioning catalytically active amino acid side-chains in close proximity to other functional groups, such as backbone amides, that might also interact with substrates through H-bonding.[13] Figure 1 highlights three representative asymmetric reactions developed in our laboratory that are catalyzed by such β-turn-containing

Received: November 1, 2016
Published: December 28, 2016

© 2016 American Chemical Society

DOI: 10.1021/jacs.6b11348
J. Am. Chem. Soc. 2017, 139, 492−516

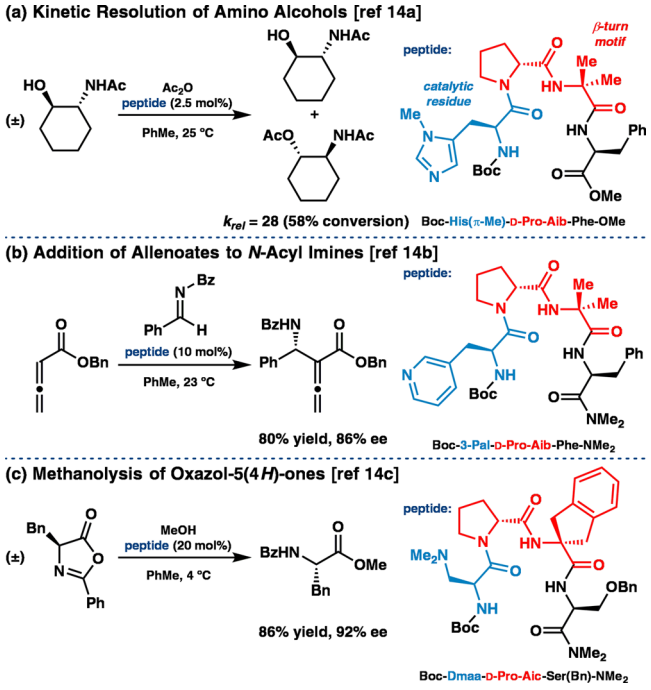

Figure 1. Examples of asymmetric reactions catalyzed by β-turn-containing peptides, including (a) a kinetic resolution of amino alcohols,[14a] (b) an addition of allenoates to *N*-acyl imines,[14b] and (c) a methanolytic dynamic kinetic resolution of oxazol-5(4*H*)-ones.[14c]

peptides.[14] In each case, experimental data support the designation of a β-turn secondary structure.

The potential homology among substructure elements in proteins and much smaller peptide-based catalysts has consistently influenced our studies. For context in terms of structure,[15] it has been estimated that up to 25% of all residues in proteins are involved in β-turns.[3,10] Accordingly, this scaffold has been studied in numerous contexts spanning biology and chemistry.[16] In fact, a major focus in the field of peptidomimetics has been to develop β-turn mimics, or compounds that exhibit turn-like conformations but whose biological functions are modulated in some way.[17] β-Turns have been historically classified according to the ϕ and ψ dihedral angles of the loop-region (ϕ,ψ(i+1) and ϕ,ψ(i+2), Figure 2a).[3,10] The most common β-turn motifs in proteins are types I and II, though the so-called "mirror image" turns, types I′ and II′, predominate in β-hairpin substructures (Figure 2b).[3] β-Turns of types I/I′ are related to types II/II′ by a plane-flip of the loop-region amide, a relatively low-barrier process that is known to interconvert turn-types in proteins.[18] Among all of the common turn-types, the possibility exists for a ten-membered ring H-bond between N−H(i+3) and O(i). While the folding of a peptide into a β-turn is a multifaceted process driven in part by local torsional preferences, interstrand H-bonding can offer additional stabilization of the turn.[3,10,11] This is especially apparent in studies of β-hairpins, wherein the additional 14-membered ring H-bond between N−H(i) and O(i+3) reinforces close interstrand distances, often less than 7 Å between the α-carbons of the i and i+3 residues, and perpetuate β-sheet-type structures in proteins.[12,19]

All of the β-turn-containing peptide catalysts shown in Figure 1, and many others not depicted,[20] possess a two-residue Pro-Xaa loop-region, where Pro is D- or L-proline, and Xaa is a locally achiral, α,α-disubstituted amino acid. Our initial decision to explore Pro-containing catalysts was built upon the established propensity of Pro to restrict the conformational space available to the peptide by virtue of its pyrrolidine ring.[21] In fact, Pro is the most frequent residue to occur at the i+1 position of type I and II β-turns in proteins.[3] The potential for control of conformation through defined stereochemical alteration of the i+1 Pro residue, as explored by Gellman and others, has proven particularly powerful in catalyst design.[11a,22] For example, replacement of L-Pro with D-Pro in an otherwise L-homochiral turn sequence often changes not only the turn sense from type II to type II′, but also shifts the conformational equilibrium to favor the β-hairpin form (Figure 2c). The hairpin conformer is not typically favored in homochiral oligopeptides, which instead tend to equilibrate between β- and γ-turn forms.[11a,23] In addition, Toniolo and co-workers have thoroughly investigated the use of achiral, α,α-disubstituted amino acids in short peptide sequences.[24] These residues are more conformationally restricted than glycine, the most frequent residue found at the i+2 position of β-turns in

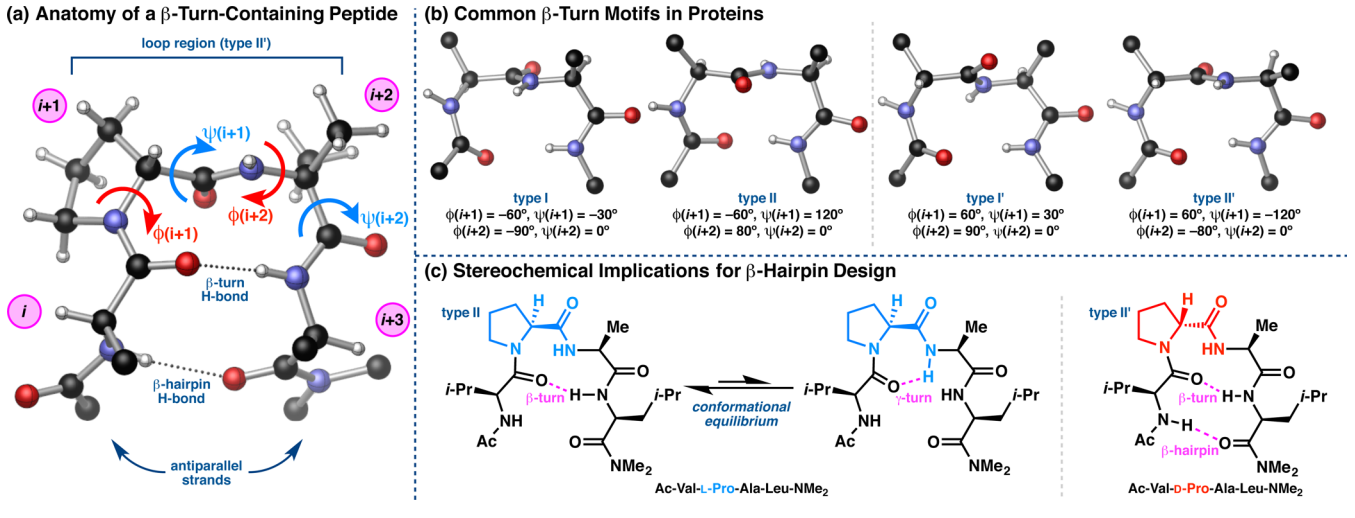

Figure 2. (a) Pertinent features of a β-turn-containing peptide. (b) Canonical β-turn-types most frequently observed in protein crystal structures.[3] (c) The work of Gellman and co-workers showed that heterochiral β-turn sequences are conformationally more apt to adopt β-hairpin structures relative to homochiral sequences.[11a]

DOI: 10.1021/jacs.6b11348
J. Am. Chem. Soc. 2017, 139, 492−516

proteins,[3] and they have been found to bias Pro-Xaa β-turns into the type II/II′ regime when incorporated at the i+2 position.[25]

Application of these important principles allowed the development of highly enantioselective peptide-based catalysts biased toward type II (Pro-Xaa) or type II′ (D-Pro-Xaa) β-turns with seemingly limited conformational flexibility. The large number of effective catalysts that have been developed within this motif has also raised questions regarding the possibly "privileged" nature of the Pro-Xaa turn sequence for asymmetric catalysis (Figure 1).[14,20,26] Additional catalysts based upon this structural motif are emerging with some regularity.[27] Even so, our resolution in catalyst design has remained relatively low, as the connection between subtle changes in peptide sequence and their effect on enantioselectivity has rarely been clear. Moreover, as we will detail below, the conformational mobility of intentionally biased sequence space has also proven greater than our initial intuition suggested.

For context in terms of function, we recently developed a catalytic, atroposelective bromination of 3-arylquinazolin-4(3*H*)-ones (**1**), providing access to highly enantioenriched tribromides (**2**, eq 1).[28a] Peptide **3**, which possesses a tertiary

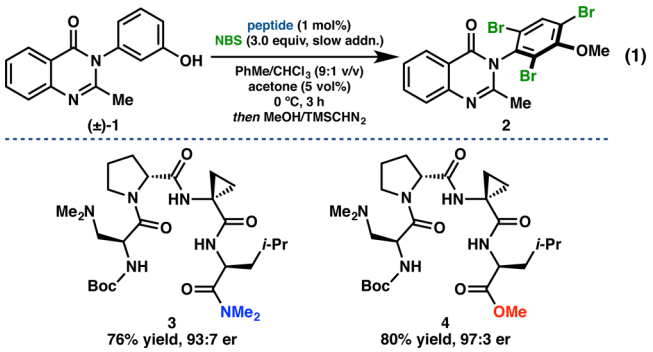

amine-containing L-β-dimethylaminoalanine (Dmaa) residue at the i-position and a D-Pro-Acpc turn-motif, emerged as the lead catalyst for this transformation from an initial library of 24 sequences biased toward presumed type II′ β-turns. Upon expanding our catalyst library to 54 total peptides, we discovered an improved catalyst (**4**) that differed from **3** only in the *C*-terminal cap, and yet it delivered **2** in 97:3 er at only 1 mol % loading (eq 1).[28b] Motivated by a desire to better understand the delicate interplay between peptide structure and enantioselectivity in this reaction, we sought to study structural aspects of our bromination catalyst library using X-ray crystallography and NMR spectroscopy. It is this library that most comprehensively revealed the structural heterogeneity available to peptide-based catalysts of this type.

We report herein a detailed structural study of 35 Pro-Xaa-containing peptides, each of which proved suitable for analysis in the solid state using single crystal X-ray diffraction. Crystallographic data on such catalytic tetrapeptides have been limited in previous years. Of the sequences examined, X-ray crystal structures of only six have been reported previously (**3**, **4**, **34**−**37**, Chart 1).[9,28,29] The 29 newly reported peptides (**5**−**33**, Chart 1) represent a substantial increase in the number of small molecule, β-turn-containing crystal structures in the Cambridge Structural Database (CSD).[30] Furthermore, we have observed an unexpected frequency of polymorphism and symmetry-independent conformational isomerism. Thus, the total number of peptide conformational states we describe sums to 53. In Chart 1, we denote in red the number of discrete states observed for a given sequence. The combination of X-ray crystallography, DFT computational studies, and solution-phase NMR spectroscopy has also helped us to understand better the conformational effects associated with changes to the primary sequence. Of particular interest were the effects of various i+2 substitutions on secondary structure, since changes to this particular residue often perturb the enantioselectivity significantly in peptide-catalyzed reactions. *In general, a wider range of ground state structures was observed than might have been expected based on standard design principles.*[3,11a] Focusing on ground state structural issues alone, the conformational diversity that may be reasonably populated within the generic β-turn framework is striking.[31] Conformations that span the canonical β-turn classifications, and even populate their boundaries, have been observed. These findings are consistent with multiple accessible states, which intersects with ongoing studies regarding the importance of catalyst dynamics.[32] Critically, the results of this study offer opportunities to expand our understanding of the connection between catalyst structure and enantioselectivity outcomes. As is well appreciated, these issues present tremendous challenges for combined experimental and computational approaches that, together, promise to advance our understanding of the structure−function continuum for catalytic reactions.[33]

RESULTS AND DISCUSSION

Conformational Polymorphs and Pseudopolymorphs.

Crystallographic Analysis of Peptide ***3***. The observation of three distinct conformations of peptide **3** in the solid state (Figure 3) stimulated an aggressive inquiry into the potential generality of the phenomenon. Conformers **3a** and **3b** were identified within the same asymmetric unit,[28] and both are characterized as type II′ β-hairpins on the basis of their loop-region dihedrals, ϕ,ψ(i+1) and ϕ,ψ(i+2), and the presence of N−H(i+3)···O(i) and N−H(i)···O(i+3) intramolecular H-bonds. Conformer **3c**, on the other hand, was identified within a polymorphic crystal grown under nearly identical conditions, and yet its structure most closely resembles a type I′ β-turn when considering the ϕ and ψ dihedrals of the i+1 and i+2 positions and the N−H(i+3)···O(i) H-bond. Another ten-membered ring N−H(i+2)···O(i−1) H-bond delineates a second β-turn within the same tetrameric framework. The i and i+1 residues comprise the loop-region of this *N*-terminal β-turn, which is characterized by type II ϕ and ψ dihedrals. This sequential, II/I′ double β-turn motif provides a nascent $3_{10}'$-helical structure to **3c**, although the sequence is too short to constitute a true helix (Tables S4.04 vs S4.05).[34] Nonetheless, the observation of **3c** was initially unexpected for a D-Pro-Xaa-containing sequence, which is often presumed to nucleate a type II′ β-hairpin geometry.[3,11] A structural overlay of the conformers of **3** highlights the differences between the prehelical **3c** and **3a**,**b** (Figure 3).

Although **3a** and **3b** broadly classify into the same structural motif, there are a number of differences between the two structures. For instance, the ψ(i+1) value of **3a** is nearly 26° contracted relative to that of **3b**. This is possibly a manifestation of the incipient N−H(i+2)···O(i) intramolecular H-bond in **3a**. This type of H-bond is characteristic of a γ'-turn,[23] though the comparatively long N···O length of 3.029(6) Å and the acute N−H···O angle of 96(4)° suggest that the β-turn geometry is favored. Perhaps the most prominent

DOI: 10.1021/jacs.6b11348
J. Am. Chem. Soc. 2017, 139, 492−516

Chart 1. Peptides Analyzed by X-ray Crystallography

3 Boc-Dmaa-D-Pro-Acpc-Leu-NMe_2 (3)
4 Boc-Dmaa-D-Pro-Acpc-Leu-OMe (5)
5 Boc-Cys(Ph)-D-Pro-Acpc-Leu-OMe
6 Boc-Leu-D-Pro-Acpc-Leu-OMe
7 Boc-Dmaa-D-Pro-Acpc-Gly-OMe (2)
8 Boc-Dmaa-D-Pro-Acpc-Nle-NMe_2
9 Boc-Dmaa-D-Pro-Acpc-Val-NMe_2
10 Boc-Dmaa-D-Pro-Acpc-Val-OMe
11 Boc-Dmaa-D-Pro-Acpc-Chg-NMe_2
12 Boc-Dmaa-D-Pro-Acpc-Phe-NMe_2
13 Boc-Dmaa-D-Pro-Acpc-Phe-OMe
14 Boc-Dmaa-D-Pro-Acpc-D-Phe-NMe_2
15 Boc-Dmaa-Pro-Acpc-Leu-OMe

16 Boc-Dmaa-D-Pro-Acbc-Leu-NMe_2 (3)
17 Boc-Dmaa-D-Pro-Acbc-Leu-OMe (2)

18 Boc-Dmaa-D-Pro-Cle-Leu-OMe (2)

19 Boc-Dmaa-D-Pro-Aic-Leu-OMe (2)
20 Boc-Dmaa-D-Pro-Aic-D-Phe-NMe_2 (2)
21 Boc-Dmaa-Pro-Aic-Leu-OMe (2)

22 Boc-Dmaa-D-Pro-Achc-Leu-OMe (2)
23 Boc-Cys(Ph)-D-Pro-Achc-Leu-OMe

24 Boc-Dmaa-D-Pro-Aib-Leu-NMe_2
25 Boc-Dmaa-D-Pro-Aib-Leu-OMe
26 Boc-Dmaa-D-Pro-Aib-Val-OMe
27 Boc-Dmaa-D-Pro-Aib-Phe-OMe
28 Boc-Dmaa-D-Pro-Aib-3-Pal-NMe_2
29 Boc-Dmaa-D-Pro-Aib-2-Thi-NMe_2 (2)
30 Boc-Dmaa-Pro-Aib-Leu-OMe

31 Boc-Dmaa-D-Pro-Ala-Phe-OMe
32 Boc-Dmaa-D-Pro-Phe-Leu-NMe_2 (2)

33 Boc-Dmaa-D-Pro-Gly-Leu-OMe (2)

34 Boc-Keto-D-Pro-Aib-Phe-OMe
35 Boc-Phe-Pro-Aib-(*R*)-α-Mba
36 2-Msa-Pro-D-Val-(*R*)-α-Mba
37 Boc-His(τ-Bn)-Pro-Aib-(*R*)-α-Mba

* *Values in parentheses indicate the number of discrete states observed crystallographically.*

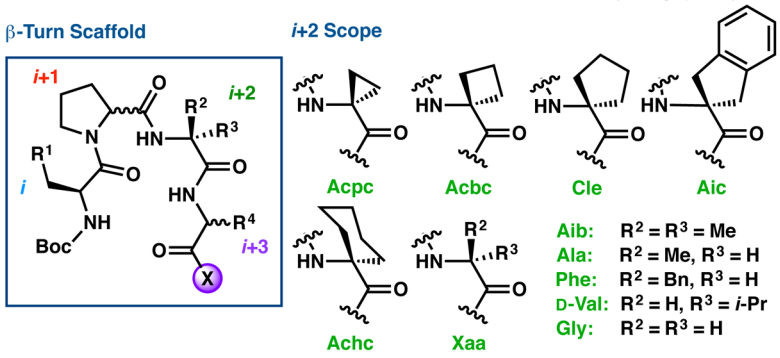

Abbreviations: Boc, *tert*-butylcarbamate; Dmaa, L-β-dimethylaminoalanine; Acpc, 1-amino-cyclopropyl-1-carboxamide; Acbc, 1-aminocyclobutyl-1-carboxamide; Cle, cycloleucine; Aic, 2-aminoindane-2-carboxamide; Achc, 1-aminocyclohexane-1-carboxamide; Aib, α-aminoisobutyramide; 3-Pal, L-β-3-pyridylalanine; 2-Thi, L-β-2-thienylalanine; Keto, (*S*)-2-amino-4-oxohexanoic acid; 2-Msa, (*S*)-2-methylsuccinic acid.

difference, aside from the orientation of the *i* and *i*+3 side-chains, is the degree of backbone bending at the *C*- and *N*-terminal residues. The termini of conformer **3a** bend approximately 66° from the plane defined by the α-carbons of the *i*, *i*+1, *i*+2, and *i*+3 residues, while that of **3b** bends only 41° (Table S4.12 and associated figure). Thus, conformer **3a** is more bent than **3b**, resulting in a more compact structure. Another feature that differentiates these two conformers is the degree of twisting, as measured by the virtual dihedral angle (ϖ) defined by the four α-carbons (Table S4.14 and associated figure).[35] Conformers **3a** and **3b** twist in opposite directions, with ϖ measuring 9.4° and −21.3°, respectively, suggesting that both twist-senses are accessible to peptide **3**. These details provide insight into the range of conformations available to short peptides of the same overall structural class.

A closer analysis of conformer **3c** also reveals some structural nuances (Figure 3). Though $\phi,\psi(i+1)$ and $\phi,\psi(i+2)$ classify the central turn-motif as a type I′ turn, the dihedral values are distorted from their canonical values.[3] For instance, $\psi(i+1)$ is nearly 15° contracted, while $\phi(i+2)$ and $\psi(i+2)$ are wider than predicted by 19° and 15°, respectively. It is possible that these deviations may be caused by the N−H(*i*+2)···O(*i*−1) β-turn H-bond, which is significantly shorter than the central N−H(*i*+3)···O(*i*) H-bond of **3c** (as well as both of the H-bonds in **3a** and **3b**). Formation of this particularly favorable H-bond likely counterbalances the torsional distortions in the backbone. The *i* and *i*+1 residues define the loop-region of the *N*-terminal β-turn. In this case, the N−H(*i*+3)···O(*i*) H-bond likely causes some deviations from the ideal type II torsional potentials. The second residue of a type II β-turn typically possesses ϕ values of 80°. However, this value is contracted by nearly 16° in **3c**, a direct consequence of the pyrrolidine ring of D-Pro, which typically locks ϕ at 60 ± 10°. The pronounced twist of **3c** (ϖ = −71.5°) reflects the prehelical nature of the sequential double β-turn motif (Table S4.16).

In order to gain insight into the degree to which crystal packing forces might affect the geometries and to assess the energy differences ($\Delta H°$ and $\Delta G°$) between the conformers, we optimized the crystallographic coordinates of **3a**−**c** using DFT (see the Supporting Information for details).[36] We found that the loop-regions of the DFT-optimized structures are nearly coincident with their respective X-ray crystal structures. However, the computed structures showed deviations in the *i* and *i*+3 residues, especially with respect to the side-chains (Figure 4). In the case of **3b**, geometry optimization causes the backbone to bend such that it more closely resembles that of **3a**. In fact, the optimized structures of **3a** and **3b** overlay with a backbone RMSD of only 0.24 Å; the only major differences occur in the side-chains. Optimization of conformer **3c** produces a structure in which the loop-region dihedrals of both β-turns have approached their canonical values, and the *N*-terminal carbamate has torqued about $\phi(i)$ to lengthen the N−H(*i*+2)···O(*i*−1) β-turn H-bond. This result is consistent with our hypothesis that formation of the N−H(*i*+2)···O(*i*−1) H-

DOI: 10.1021/jacs.6b11348
J. Am. Chem. Soc. 2017, 139, 492−516

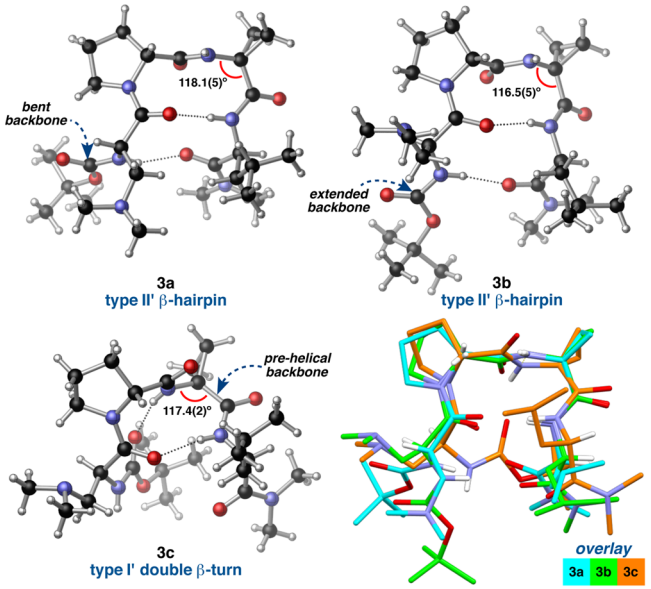

	Loop Dihedrals				H-Bond Lengths		
	$\phi(i+1)$	$\psi(i+1)$	$\phi(i+2)$	$\psi(i+2)$	N(i+3)···O(i)	N(i)···O(i+3)	N(i+2)···O(i−1)
3a	63.6(6)°	−113.0(6)°	−77.2(7)°	−3.7(8)°	2.952(6) Å	2.906(6) Å	n/o
3b	62.9(7)°	−138.7(5)°	−78.1(7)°	−5.3(8)°	2.937(6) Å	2.968(5) Å	n/o
3c	64.3(2)°	15.2(2)°	71.9(2)°	14.9(3)°	3.022(2) Å	n/o	2.871(2) Å

Figure 3. Three distinct conformations of peptide **3** with relevant crystallographic measurements. A structural overlay highlights the differences among the conformers (loop RMSD (**3a**/**3b**) = 0.14 Å, loop RMSD (**3a**/**3c**) = 0.74 Å).

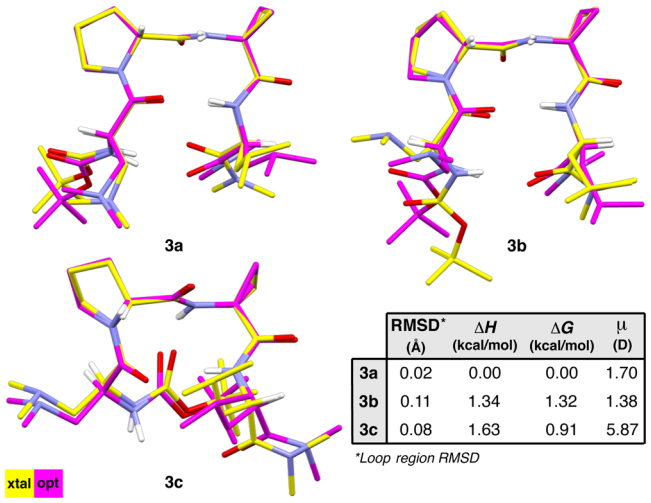

	RMSD* (Å)	ΔH (kcal/mol)	ΔG (kcal/mol)	μ (D)
3a	0.02	0.00	0.00	1.70
3b	0.11	1.34	1.32	1.38
3c	0.08	1.63	0.91	5.87

*Loop region RMSD

Figure 4. Three solid-state conformations of peptide **3** were optimized using DFT at the M06-2X/6-311++G(2d,3p)//B3LYP/6-31+G(d,p) level of theory.

bond is coupled to the conformational distortion of the backbone. It is notable that **3c** does not converge to a type II′ β-hairpin, which solidifies its characterization as a conformational polymorph of **3a**,**b**.[37] In terms of relative energies, conformer **3a** was found to be the lowest-energy conformer, while the prehelical **3c** was higher by only 0.91 kcal/mol. Conformer **3c** has the highest relative enthalpy, which suggests that there is some entropic benefit to occupying the prehelical geometry. It also has a significantly larger dipole moment (μ) than either of the β-hairpin conformers, suggesting that its population might be sensitive to solvent. Surprisingly, conformer **3b** was 0.41 kcal/mol higher in energy than **3c**, despite the tight overlay between **3a** and **3b**. This is possibly due to the orientation of the i and i+3 side-chains in **3b**.

NMR Analysis of Peptide ***3***. We next sought to compare the solution conformational profile of **3** to its observed solid-state structures. The solution structure of peptide **3** has been studied extensively in our laboratory. For example, we have recently reported an NMR-derived structure of **3** that was computed using a NOE-restrained simulated annealing/DFT protocol.[28b] This treatment produced a solution structure of **3** that was a hybrid of its solid-state conformers, **3a**−**c**. A more comprehensive analysis presented herein supports these findings and is predicated on a NMR-based, three-pronged approach: (1) three-bond couplings between the amide- and Cα-protons ($^3J_{NH-H\alpha}$) of the i and i+3 residues were extracted from ^{1}H NMR spectra and used to calculate $\phi(i)$ and $\phi(i+3)$ (Table S5.40 and Figure S5.15);[38] (2) the relative chemical shifts and peak widths of the NH(i), NH(i+2), and NH(i+3) signals were compared to assign their H-bonded state (Tables S5.41−S5.43);[39] and (3) NOE contacts from two-dimensional ^{1}H−^{1}H-NOESY spectra were analyzed for information about through-space interactions.[40] All NMR analyses were performed using benzene-d_6 (C_6D_6) as the solvent in order to simulate the reaction conditions (9:1 PhMe/$CHCl_3$) with fewer residual solvent peaks that could complicate analysis. Comparable enantioselectivities were obtained upon substitution of benzene for toluene in the catalytic bromination of **1** (eq 1).[28] Concentrations of 0.01 M with respect to peptide were used, which is 10 times more concentrated than the reaction conditions. However, we previously demonstrated that this concentration is still below the aggregation limit for peptides of this class.

Our investigation of **3** in solution (0.01 M, C_6D_6, 25 °C) provided data consistent with $\phi(i)$ = −86° or −154° and $\phi(i+3)$ = −95° or −145° based on the $^3J_{NH-H\alpha}$ (Table S5.40). Based on the empirically derived cutoffs, these dihedral values do not preclude any specific secondary structure. Relative to other peptides with similar primary sequences, the NH(Leu) and NH(Dmaa) signals appear at downfield chemical shifts, while that of NH(Acpc) appears at a relatively upfield shift (Table S5.41). These data suggest that NH(Leu) and NH(Dmaa) are both involved in intramolecular H-bonds, while NH(Acpc) is exposed to the solvent. Five especially interesting cross-peaks in the NOESY spectrum of **3** are indicative of the following through-space interactions: NH(Dmaa) ↔ NH(Leu), NH(Acpc) ↔ NH(Leu), NH(Dmaa) ↔ NMe_{trans}(Leu), NH(Leu) ↔ α(D-Pro), and β(Dmaa) ↔ β(Leu). A particularly strong NH(Acpc) ↔ α(D-Pro) NOE was also observed (Figure S5.01). These interactions, in conjunction with the proposed intramolecular H-bonds, point to a type II′ β-hairpin structure in solution, much like **3a**/**3b**. However, the presence of NH(Acpc) ↔ δ(D-Pro) and Boc(Dmaa) ↔ β(Acpc) NOE correlations provides evidence that a prehelical conformer much like **3c** is populated to a lesser extent in solution. Moreover, the calculated $\phi(i)$ and $\phi(i+3)$ dihedrals are also consistent with nonhairpin β-turn and prehelical conformations, further supporting our assertion that **3**, and other peptides of this type, may populate multiple conformations in solution.

Crystallographic Analysis of Peptide ***16***. We also observed three, distinct, solid-state conformations of peptide **16**, a homologue of **3** in which the i+2 position is substituted with an Acbc residue (Figure 5). Type II′ β-hairpins **16a** and **16b** were

DOI: 10.1021/jacs.6b11348
J. Am. Chem. Soc. 2017, 139, 492−516

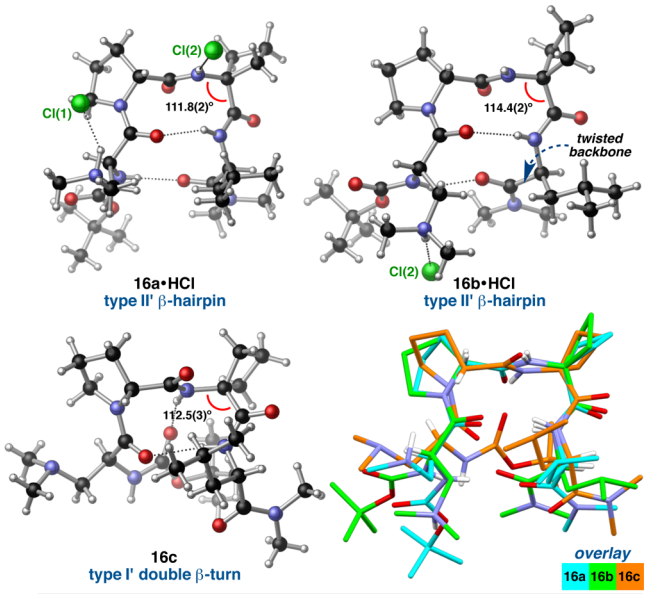

	Loop Dihedrals				H-Bond Lengths		
	ϕ(*i*+1)	ψ(*i*+1)	ϕ(*i*+2)	ψ(*i*+2)	N(*i*+3)···O(*i*)	N(*i*)···O(*i*+3)	N(*i*+2)···O(*i*−1)
16a	71.0(3)°	−128.0(3)°	−71.0(3)°	−20.6(4)°	2.995(4) Å	2.859(4) Å	n/o
16b	67.9(3)°	−116.6(3)°	−66.8(4)°	−14.6(4)°	3.190(4) Å	2.805(4) Å	n/o
16c	65.7(4)°	14.2(5)°	67.1(4)°	28.7(5)°	3.106(4) Å	n/o	2.891(4) Å

Figure 5. Three distinct conformations of peptide **16** with relevant crystallographic measurements. A structural overlay highlights the differences among the conformers (loop RMSD (**16a**/**16b**) = 0.11 Å, loop RMSD (**16a**/**16c**) = 0.74 Å).

identified within the same unit cell, while type I′ double *β*-turn **16c** was found in a pseudopolymorphic crystal. Despite the fact that the crystallization samples were prepared under nearly identical conditions, the single crystals that gave rise to **16a**,**b** and **16c** are not truly polymorphic due to the presence of 2 equiv of HCl in the unit cell of the former.[41] In both **16a** and **16b**, the Dmaa residues appear to be protonated at the tertiary amine moiety, and the resulting ammonium ions are engaged in intermolecular H-bonds with each of the two chloride counterions. Conformer **16a**, however, is also associated with the other chloride via an intermolecular H-bond donated from the N−H(*i*+2). It is possible that this intermolecular H-bond accounts for the wider *ψ*(*i*+1) in **16a**, though the sampling of an N−H(*i*+2)···O(*i*) H-bond in **16b** may also contribute to the difference.

As with **3a** and **3b**, type II′ *β*-hairpins **16a** and **16b** exhibit significant variation despite sharing the same secondary structural motif. For example, the *i*+2 main-chain angles (*τ*) differ substantially between **16a** and **16b**, with that of the former measuring 111.8(2)° compared to 114.4(2)° in that of the latter (Figure 5). We initially wondered if this difference might be related to the orientation of the cyclobutane ring.[42] In **16a**, the *i*+2 cyclobutane ring puckers away from the D-Pro residue, whereas it puckers toward the D-Pro residue in **16b**. Structure **16c** shares the same pucker direction as **16a** and has a similar *τ*(*i*+2) of 112.5(3)°. However, the difference in *τ*(*i*+2) may also be coupled to the incipient N−H(*i*+2)···O(*i*) *γ*′-turn H-bond in **16b**, an orientation that might exacerbate the electrostatic repulsion between the N−H(*i*+2) and N−H(*i*+3) *σ*-bonds, and thereby widen *τ*(*i*+2) relative to **16a**.[43] This hypothesis was further substantiated by DFT optimization of **16a** and **16b** without the associated HCl equivalents. The optimized structures both exhibit *τ*(*i*+2) values >114°, and while the loop-region of **16b** remains nearly constant, that of **16a** becomes more like **16b** and begins to adopt a *γ*′-turn H-bond (Figure 6). Another distinguishing feature between **16a** and **16b** is the backbone twist. Much like **3a** and **3b**, these two conformers twist in opposite directions, with *ϖ* measuring −7.9° and 17.8°, respectively (Table S4.14). The *i* and *i*+3 side-chains of **16a** and **16b** are also oriented differently, with **16a** adopting a more compact arrangement.

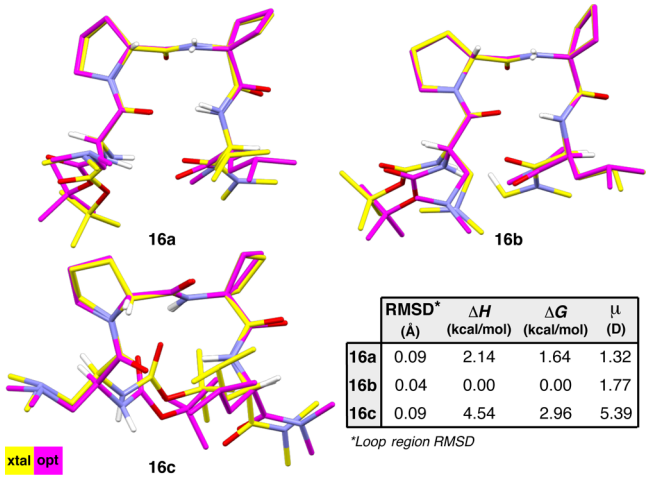

	RMSD* (Å)	Δ*H* (kcal/mol)	Δ*G* (kcal/mol)	μ (D)
16a	0.09	2.14	1.64	1.32
16b	0.04	0.00	0.00	1.77
16c	0.09	4.54	2.96	5.39

*Loop region RMSD

Figure 6. Three solid-state conformations of peptide **16** were optimized using DFT at the M06-2X/6-311++G(2d,3p)//B3LYP/6-31+G(d,p) level of theory.

Much like **3c**, conformer **16c** is characterized by a prehelical, type I′ *β*-turn secondary structure that is underdocumented for a D-Pro-Xaa sequence (Figure 5). Many of the structural characteristics of **3c** are mirrored in **16c**; the two structures overlay with a backbone RMSD of only 0.12 Å. The primary difference between the two structures is the *ψ*(*i*+2) value, which measures nearly twice as wide in **16c** at 28.7(5)°. It is possible that this difference is related to the torquing of the cyclobutane ring away from the central *β*-turn. The 23° deviation of *ϕ*(*i*+2) from the ideal values may also stem from this torquing effect. These values of *ϕ*,*ψ*(*i*+2) are at the very boundary of what would canonically be considered a type I′ *β*-turn,[3] though *ϕ*,*ψ*(*i*+1) are in accordance with this assignment.

It is interesting to note that the comparisons among **3a**−**c** and **16a**−**c** appear to be analogous, despite the presence of HCl salts for **16a** and **16b**. While this is certainly a caveat worth considering, we do not expect that protonation of the peptides and association of the chloride counterion necessarily affects the structure in a way that might devalue these comparisons. Wennemers and co-workers recently reported that separate crystal structures of a short peptide and its corresponding TFA salt did not deviate to any significant extent.[44] To probe these issues further, we omitted the HCl equivalents and optimized structures **16a** and **16b** using DFT. The optimized geometries overlaid closely with the corresponding X-ray crystal structures (loop RMSDs < 0.10 Å, Figure 6). Thus, the presence of the HCl appears not to alter the structures significantly. Furthermore, DFT optimization of **16a**−**c** also allowed us to assess the relative energies of the three structures. In this case, conformer **16b** was found to be significantly lower in energy than the others. Prehelical **16c** is significantly more disfavored relative to the *β*-hairpin geometries in the context of peptide **16** than it is in peptide **3** (Figure 4). This underscores an influence

DOI: 10.1021/jacs.6b11348
J. Am. Chem. Soc. 2017, 139, 492−516

of the i+2 residue on the conformational energy landscape of these peptides.

NMR Analysis of Peptide **16**. Solution NMR data were acquired for peptide **16** to provide insight into its conformational profile (0.01 M, C_6D_6, 20 °C). In the ^{1}H NMR spectrum of **16**, the N*H*(Dmaa) signal appears as a broad singlet, implying a $\phi(i)$ dihedral of approximately −30°. It is difficult to draw definitive conclusions based on this $\phi(i)$, as the broadness of the resonance might point to conformational averaging at this residue. On the other hand, the $^3J_{NH-H\alpha}$ of N*H*(Leu) is consistent with $\phi(i+3)$ values of either −96° or −143° (Table S5.40), which are most in-line with the β-turn or hairpin conformations (i.e., **16a**/**16b**) and are on the upper limit of what might be expected for a prehelical, type I′ β-turn assignment (i.e., **16c**). Compared to peptide **3**, the chemical shifts of the N*H*(Leu) and N*H*(Dmaa) signals are upfield-shifted, while that of the N*H*(Acbc) occurs significantly further downfield (Table S5.41). Taken together, these relative chemical shift data provide evidence for a conformation in which: (1) N*H*(Acbc) is involved in a strong, intramolecular H-bond; (2) N*H*(Dmaa) is mostly solvent-exposed; and (3) N*H*(Leu) samples multiple H-bonded states on the NMR time-scale. In terms of through-space interactions, a strong N*H*(Acbc) ↔ α(D-Pro) NOE is present in the NOESY spectrum of **16**. This correlation typically supports type II′ loop dihedrals, much like **16a**/**16b**. However, the absence of cross-strand NOEs perhaps intimates that the structure is in-flux between multiple conformers (Figure S5.05). These cumulative data provide evidence that supports a γ'-turn that is perhaps in equilibrium with the nonhairpin β-turn form. Conformer **16b** shows some characteristics of an incipient γ'-turn conformation in the solid state (Figure 5).

Packing Polymorphs. *Crystallographic Analysis of Peptide* **4**. While peptides **3** and **16** exhibit multiple solid-state conformations that are significantly different from one another in their polymorphic or pseudopolymorphic crystal structures, we have also observed cases in which the degree of structural variation is subtler. For example, two polymorphic crystal structures of peptide **4** give rise to five distinct states, all of which are similar to one another (Figure 7). The initial crystal structure provided **4a**, a type I′ double β-turn similar to both **3c** and **16c**. Upon recrystallization of peptide **4** under nearly identical conditions, a polymorphic unit cell was found to contain four symmetry-independent molecules (**4b**–**e**) that adopt secondary structures similar to that of **4a**. As such, crystal structures **4b**–**e** may be described as a packing polymorph of **4a**.[37] An overlay of **4a**–**e** reveals that the five states are remarkably consistent across the i+1 and i+2 residues, with loop-region RMSDs (relative to **4a**) of <0.03 Å (Figure 7a). The loop dihedral with the most variation is $\psi(i+1)$, which varies from 12.6(6)° to 21.8(6)° across the set. Unlike the loop-regions, the termini of **4a**–**e** vary more significantly. The *C*-terminus, in particular, shows a range of conformations in both the backbone and the Leu side-chain. The principle metric of this variation is $\phi(i+3)$,[15] which ranges from −65.1(6)° in **4c** to −135.7(4)° in **4e** with an average of −101.4 ± 27.2° (Table S4.03). The high standard deviation of the mean $\phi(i+3)$ value is a reflection of the conformational heterogeneity at the *C*-terminus. We note that $\psi(i+3)$ also varies across **4a**–**e**, but to a lesser extent, ranging from 150.4(4)° in **4b** to 178.3(4)° in **4e**. The variation observed in the i+3 side-chain appears to be coupled to the backbone deviations, as the side-chain dihedral $\chi_1(i+3)$ remains fairly constant across **4a**–**d**,[15] only ranging from −58.3(5)° in **4d** to −67.2(5)° in **4c** (Table S4.32). The exception is conformer **4e**, in which $\chi_1(i+3)$ measures 57.3(5)°. Positive *gauche* (g^+) values of χ_1 are quite infrequent at the i+3 position of these β-turn-containing tetrapeptides, since side-chains oriented in this way incur two destabilizing *gauche* interactions from the main-chain.

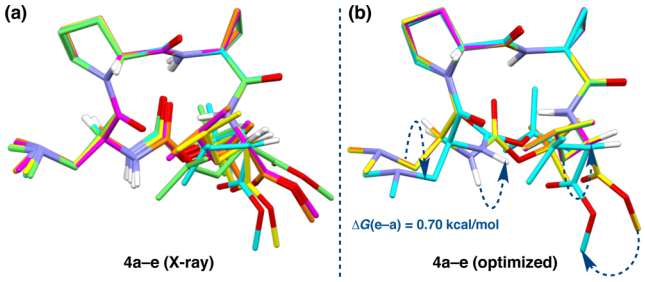

	Loop Dihedrals				H-Bond Lengths		RMSD vs. 4a	
	ϕ(*i*+1)	ψ(*i*+1)	ϕ(*i*+2)	ψ(*i*+2)	N(*i*+3)···O(*i*)	N(*i*+2)···O(*i*−1)	xtal	opt
4a	62.4(3)°	17.7(3)°	72.7(4)°	11.9(5)°	3.096(3) Å	2.964(3) Å	n/a	n/a
4b	61.1(5)°	21.8(6)	71.5(5)°	11.4(6)°	3.045(4) Å	2.958(4) Å	0.02 Å	0.00 Å
4c	63.8(5)°	12.6(6)°	71.7(6)°	12.3(6)°	3.008(5) Å	2.963(6) Å	0.03 Å	0.00 Å
4d	61.6(5)°	19.3(6)°	73.1(6)°	10.9(6)°	3.059(4) Å	2.914(6) Å	0.01 Å	0.00 Å
4e	62.8(5)°	13.3(6)°	74.5(6)°	15.1(6)°	3.093(5) Å	2.899(6) Å	0.02 Å	0.07 Å

Figure 7. (a) Overlay of the five solid-state conformations of peptide **4** that were identified within two polymorphic unit cells. (b) DFT Optimization of **4a**–**e** at the M06-2X/6-311++G(2d,3p)//B3LYP/6-31+G(d,p) level of theory led to two distinct families of conformers, shown overlaid. The optimized structures of **4a**–**d** were degenerate, while **4e** was found to be 0.70 kcal/mol higher energy than **4a**–**d**. Loop RMSDs are reported in the table.

Given the subtlety of the structural differences among **4a**–**e**, a pertinent question is whether each might converge to the same conformation upon minimization. As such, we optimized the crystallographic geometries of **4a**–**e** using DFT and found that **4a**–**d** converge to a single structure (Figure 7b). The optimized structure of **4e**, however, is distinct, with a small, yet nonzero, loop-region RMSD of 0.07 Å relative to **4a** (Figure S6.02) and some significant structural deviations in the termini (Figure 7b, arrows). As we observed with the DFT-optimized structures of **3c** and **16c** above, the *N*-terminal carbamates of **4a**–**e** torque about $\phi(i)$, which orients the N–H(i)s toward O(i+3) on the opposite strands; this may be coupled to the lengthening of the N–H(i+2)···O(i−1) H-bonds and the minor differences in the Dmaa side-chain of **4e** relative to **4a**–**d**. This effect is more prominent in **4e**, wherein N–H(i) is in close enough range for a *bona fide* β-hairpin H-bond to O(i+3). Minor differences in the Dmaa side-chain of **4e** relative to **4a**–**d** may be related to this pronounced torquing. The values of $\phi(i+3)$ and $\chi_1(i+3)$ observed in the crystal structure of **4e** are largely maintained after optimization, measuring −128.0° and 56.4°, respectively. The unusual *gauche* $\chi_1(i+3)$ of **4e** may be the source of the difference between the optimized structures of **4e** and **4a**–**d**, since the $\phi(i+3)$ dihedrals of **4a**–**d** were quite disparate, and yet they still converged during optimization. Conformer **4e** was found to be 0.70 kcal/mol higher in energy than **4a**–**d**, which suggests that its distorted β-hairpin geometry may be accessible to some extent at ambient temperature (Table S6.10). This energy difference is consistent with a *gauche* interaction.

NMR Analysis of Peptide **4**. We also analyzed the structure of peptide **4** in solution (0.01 M, C_6D_6, 20 °C). Using the extracted $^3J_{NH-H\alpha}$ values, we calculated $\phi(i)$ and $\phi(i+3)$ to be −30° and either −89° or −151°, respectively (Table S5.40).

DOI: 10.1021/jacs.6b11348
J. Am. Chem. Soc. 2017, 139, 492–516

Based on these criteria, no specific conformations may be excluded, but the data are most consistent with either a prehelical or nonhairpin β-turn. The relative chemical shifts of the N*H*(Leu), N*H*(Acpc), and N*H*(Dmaa) resonances point to a scenario in which all three are involved in intramolecular H-bonds (Table S5.41 and S5.42). However, the very broad peak width of the N*H*(Dmaa) signal suggests that the carbamate is experiencing different H-bonded states on the NMR time-scale (Table S5.43). The presence of N*H*(Dmaa) ↔ N*H*(Leu), Boc(Dmaa) ↔ N*H*(Leu), and Boc(Dmaa) ↔ N*H*(Acpc) NOE contacts, as well as a particularly weak N*H*(Acpc) ↔ α(D-Pro) correlation, is consistent with a prehelical, type I′ β-turn as the predominant solution conformation (Figure S5.02). In keeping with the downfield-shifted N*H*(Dmaa) signal, a type I′ β-hairpin might also be sampled to some extent.[28b] This assignment is in agreement with the turn-type observed for all five solid-state conformers **4a**−**e** (Figure 7).

Symmetry-Independent Conformers. Among the 38 different crystal structures examined in this study, we have observed multiple, distinct peptide molecules within the same unit cell in 13 instances, representing 34% of our peptide structure library (Table 1). The observation of symmetry-independent molecules is relatively uncommon among crystal structures of small organic molecules. According to Steiner's 2000 study of the CSD, 73.3% of organic crystal structures have only one formula unit per unit cell, while 15.9% have fewer and 10.8% have more than one molecule per unit cell.[45] Broken down further into compound classes, it was found that 81.6% of peptidic crystal structures have only one molecule per unit cell, while 5.2% have fewer and 13.2% have more than one molecule in the unit cell. Compared to organic molecules on the whole, peptides appear slightly more prone to this phenomenon. For example, symmetry-independent molecules have been observed in crystal structures of helical peptides acquired by Gellman and co-workers,[46] as well as in examples of β-hairpins reported by Balaram.[19] It has been proposed that flexible molecules, such as peptides, may crystallize with more than one molecule in the unit cell to achieve better packing than would be possible with only one, "awkwardly shaped" formula unit.[37] Another likely possibility is aggregation through N−H···O intermolecular H-bonding.

Table 1. Symmetry-Independent Molecules Observed

	Z′	Backbone RMSD[a] (Å)	Loop RMSD[b] (Å)	All-Atom RMSD[c] (Å)
3a,b	2	0.43	0.14	1.45
4b,c		0.27	0.04	0.54
4b,d	4[d]	0.05	0.01	0.13
4b,e		0.34	0.03	0.66
7a,b	2	1.23	0.72	1.51
16a,b	2	0.52	0.11	1.10
17a,b	2	0.13	0.03	0.32
18a,b	2	0.10	0.03	0.32
19a,b	2	1.04	0.12	1.87
20a,b	2	0.33	0.05	0.97
21a,b	2	0.13	0.02	0.26
22a,b	2	0.16	0.04	0.49
29a,b	2	0.11	0.01	0.21
32a,b	2	0.37	0.05	0.78
33a,b	2	0.17	0.03	0.34
mean	~	0.39	0.11	0.80

[a] Backbone RMSD is defined for all of the main-chain atoms. [b] Loop RMSD is defined for all atoms that comprise $\phi,\psi(i+1)$ and $\phi,\psi(i+2)$. [c] All-Atom RMSD is defined for all atoms in the peptide, including sidechains. [d] Structures **4b–e** were observed within the same unit cell, and thus Z′ = 4.

In light of these findings, we were curious about the degree to which the symmetry-independent molecules we observed differ from one another and whether or not they could be considered conformers.[47] Cruz-Cabeza and Bernstein studied the correlation between crystallographic and DFT-optimized RMSDs in pairs of conformers and developed a cutoff all-atom RMSD value of 0.375 Å, above which polymorphic or symmetry-independent structures are often true conformers.[37a] Table 1 shows the 13 cases in which we observed symmetry-independent molecules and the degree to which these peptides differ from one another using three different RMSD metrics (loop, backbone, and all-atom; Tables S4.49 and S4.50). In general, loop RMSD values were found to be lower than both backbone and all-atom RMSDs between the pairs of symmetry-independent molecules. Given that all of these peptides contain Pro-Xaa β-turn motifs, it is unsurprising that the well-defined loop-regions are more coincident than the peripheral residues. Backbone RMSDs are lower than the corresponding all-atom values for similar reasons. Eight of the symmetry-independent molecules qualify as distinct conformers based on their all-atom RMSD values. This includes the cases **3a,b** and **16a,b** discussed previously, which have all-atom RMSDs of 1.45 and 1.10 Å, respectively. Similarly, structures **4b**−**e** are symmetry-independent, yet computation reveals that only **4e** may be considered a distinct conformer. Two of the remaining five instances, those of peptides **7** and **19**, are discussed below as illustrative examples of symmetry-independent conformers.

Symmetry-Independent Conformers with Different Turn-Motifs. The symmetry-independent molecules of peptide **7** show significant deviations from one another according to all three RMSD metrics (Table 1). These differences are sufficient to warrant classification as discrete conformers. Within the unit cell, conformers **7a** and **7b** interact with one another via reciprocal N−H(i)···NMe_2(i') intermolecular H-bonds (Figure 8a). Analyzing the conformers separately, it is clear that **7a** and **7b** are not only conformers of one another, but they are different β-turn-types all together. This observation is supported by the high loop RMSD of 0.72 Å between the two conformers. The loop-region ϕ and ψ dihedrals of conformer **7a** are quite close to the canonical values of a type II′ β-turn, while conformer **7b** exhibits the loop dihedrals and intramolecular H-bonding network characteristic of the prehelical, type I′ double β-turn we have observed in **3c**, **4a**−**e**, and **16c** (Figure 8b). Analogously, the deviations from the canonical type I′ β-turn observed in **7b** are attributed to the presence of the additional N−H(i+2)···O(i−1) β-turn H-bond that gives the conformer its prehelical structure. However, this H-bond is much longer and more acute than previously observed, measuring 3.256(5) Å from N(i+2)-to-O(i−1) and 127(4)° in the N−H···O angle. This nonideal H-bond may be coupled to the pronounced pyramidalization of the i+2 amide nitrogen-atom; N(i+2) deviates 0.14 Å from the plane defined by the N-substituents, which is quite significant compared to the 0.48 Å deviation in the corresponding tertiary amine moiety of the Dmaa residue.[48] On the other hand, conformer **7a** does not exist as a β-hairpin in the solid state, even though this might be expected based on its near-canonical type II′ turn-motif and stereochemical array. It is possible that the i+3 Gly residue may provide less of a bias in favor of the β-hairpin than an α-substituted residue during crystal seeding.[3] Perhaps a more

DOI: 10.1021/jacs.6b11348
J. Am. Chem. Soc. 2017, 139, 492−516

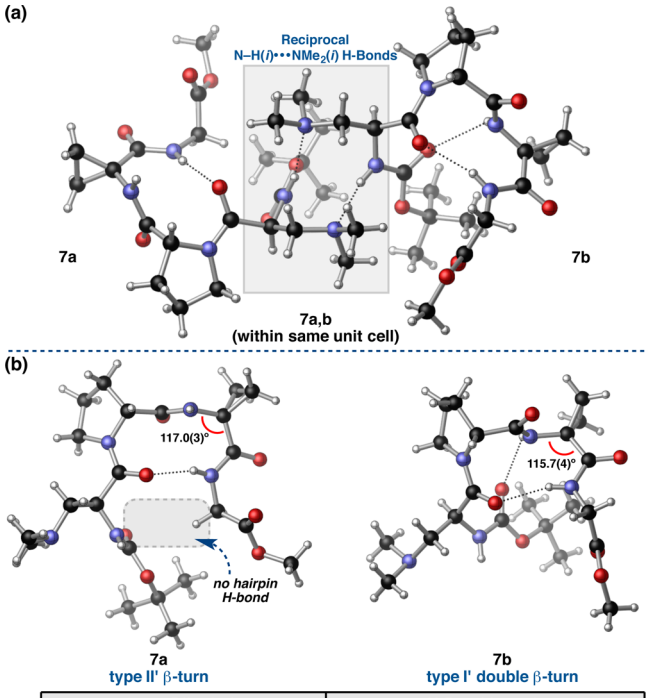

	Loop Dihedrals				H-Bond Lengths		
	ϕ(*i*+1)	ψ(*i*+1)	ϕ(*i*+2)	ψ(*i*+2)	N(*i*+3)···O(*i*)	N(*i*+2)···O(*i*−1)	N(*i*)···NMe$_2$(*i*')
7a	69.1(3)°	−123.1(3)°	−76.4(4)°	−3.0(5)°	2.804(4) Å	n/o	3.067(4) Å
7b	67.9(5)°	15.8(6)°	73.5(5)°	11.7(6)°	3.006(4) Å	3.256(5) Å	2.951(5) Å

Figure 8. (a) The two symmetry-independent conformers of peptide **7** within the unit cell. (b) Analysis of the conformers revealed two different turn-motifs, a type II′ β-turn in **7a** and a type I′ double β-turn in **7b**.

likely cause of the distortions in both **7a** and **7b** is the involvement of N−H(i) of each in intermolecular H-bonds (Figure 8a). In other words, systematic effects may favor the observed conformations to maximize packing efficiency at the expense of conformational strain.[37]

DFT optimization of **7a** and **7b** provided gas-phase geometries that coincided well with the corresponding crystal structures, especially in the loop-regions (Figure S6.03). The optimized structure of **7a** differs substantially from the crystallographic coordinates only at the i-position. The $\phi,\psi(i)$ values are, nonetheless, still atypical compared to the rest of the structure library. Optimization of **7b** results in the planarization of N(i+2) and a concomitant shortening and widening of the N−H(i+2)···O(i−1) H-bond to 3.125 Å (N···O) and 167° (N−H···O), respectively. These results lend credence to the hypothesis that the intermolecular interactions between **7a** and **7b** distort the solid-state geometries. Conformer **7b** was found to be 4.22 kcal/mol lower in energy than **7a**, reflecting both the torsional strain in the peripheral residues and the absence of a second intramolecular H-bond (Table S6.13).

In order to assess the relevance of these solid-state conformers in solution, peptide **7** was subjected to NMR analysis under the typical conditions (0.01 M, C_6D_6, 25 °C). The absence of J-coupling in the NH(Dmaa) signal suggests that the time-averaged value of $\phi(i)$ is approximately −30° (Table S5.40). However, the $^3J_{NH-H\alpha}$ of the i+3 Gly residue gives rise to $\phi(i+3)$ dihedrals of either −74° or −166°, values that are most consistent with a nonhairpin or prehelical β-turn. In addition, the downfield-shifted ^{1}H NMR resonances corresponding to NH(Gly) and NH(Acpc) provide evidence that these amides are engaged in intramolecular H-bonds; NH(Gly) most likely donates an NH(i+3)···O(i) β-turn H-bond, though the nature of the H-bond involving NH(Acpc) is more ambiguous (Tables S5.41−S5.43). The relatively upfield chemical shift of the NH(Dmaa) resonance is consistent with a solvent-exposed carbamate that is not involved in an intramolecular H-bond. A number of long-range NOEs are observed in the NOESY spectrum of **7**, including Boc(Dmaa) ↔ α(Gly), NH(Dmaa) ↔ NH(Gly), Boc(Dmaa) ↔ β(Acpc), and NH(Gly) ↔ α(D-Pro) correlations (Figure S5.03). Much like peptides **3** and **16**, a strong NH(Acpc) ↔ α(D-Pro) NOE provides evidence for type II′ loop dihedrals, although the moderately strong δ(D-Pro) ↔ NH(Acpc) and NH(Dmaa) ↔ NH(Acpc) contacts are typically associated with the prehelical, type I′ β-turn structure. Based on these data, it is likely that peptide **7** samples multiple conformations in solution, perhaps favoring a γ'-turn or a prehelical β-turn similar to **7b**.

Symmetry-Independent Conformers with the Same Turn-Motif. The symmetry-independent molecules of Aic-containing peptide **19** also differ from one another significantly, as evidenced by the all-atom RMSD of 1.87 Å between **19a** and **19b**. Unlike in the case of peptide **7**, this large global disparity stems mostly from the peripheral i and i+3 residues, as the loop RMSD is only 0.12 Å between the two conformers (Table 1). Both **19a** and **19b** are broadly characterized as type I′ double β-turns, but they do differ from the canonical geometries (Figure 9). The loop dihedrals of **19a** deviate substantially from the

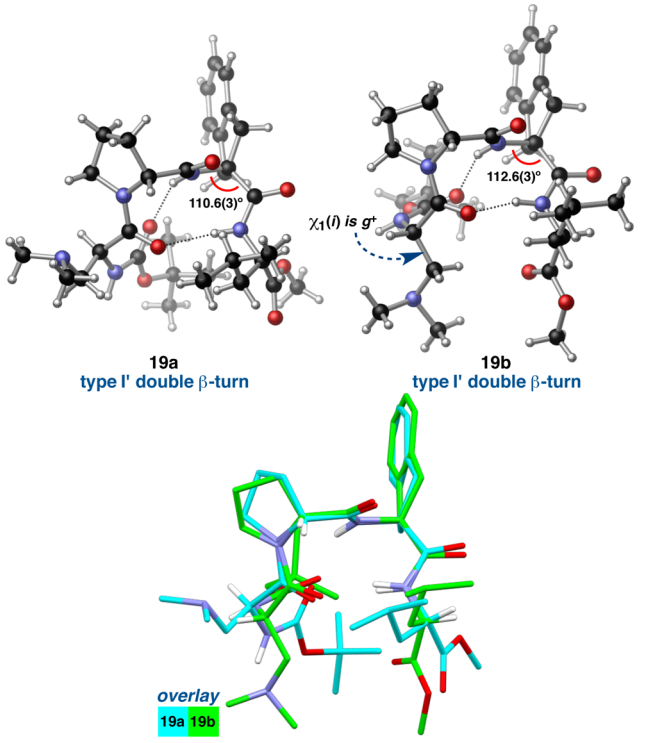

	Loop Dihedrals				H-Bond Lengths	
	ϕ(*i*+1)	ψ(*i*+1)	ϕ(*i*+2)	ψ(*i*+2)	N(*i*+3)···O(*i*)	N(*i*+2)···O(*i*−1)
19a	71.2(4)°	17.1(5)°	59.3(4)°	37.1(4)°	3.192(4) Å	3.198(4) Å
19b	62.4(4)°	29.0(4)°	67.3(4)°	17.1(4)°	2.897(4) Å	2.926(5) Å

Figure 9. Two symmetry-independent conformers of peptide **19**, both of which are classified as type I′ double β-turns. A structural overlay highlights the differences between the conformers (loop RMSD (**19a**/**19b**) = 0.12 Å).

DOI: 10.1021/jacs.6b11348
J. Am. Chem. Soc. 2017, 139, 492−516

canonical values; $\phi(i+1)$ is over 11° wider than might be expected, and $\phi,\psi(i+2)$ are both more than 30° distorted. The value of $\psi(i+1)$ also deviates from the ideal value of 30°, but this distortion is consistent across many of the type I′ double β-turns we have studied and presumably relates to the overall prehelical geometry afforded by the N−H(i+2)···O(i−1) β-turn H-bond. However, the degree of distortion in $\phi,\psi(i+2)$ is quite significant, extending beyond the classically defined boundaries (±30°) for the various turn-types (Figure 2b).[3] The N−H(i+3)···O(i−1) H-bond lengths of **19a** are also quite long, both of which measure >3.19 Å, though the N−H···O angles are both directional in favor of H-bonding (>150°). Despite these significant departures from the canonical type I′ β-turn, which likely contribute a non-negligible amount of strain in the backbone, overall **19a** resembles the other double β-turn structures we have examined (e.g., **3c**, **4a**−**e**, **16c**, and **7b**).

On the other hand, conformer **19b** has loop-region dihedrals that are in-line with the canonical values; the $\phi,\psi(i+1)$ values are very close to the established potentials, and $\phi,\psi(i+2)$ deviate to the degree we have observed previously. The two β-turn H-bonds are also much shorter than in **19a** and equally directional in terms of the N−H···O angles. However, **19b** has a rather different overall geometry owing to an unusual orientation of the *C*- and *N*-terminal residues, as shown in an overlay of **19b** with **19a** (Figure 9). We can quantify these differences by analyzing the ϕ and ψ dihedral angles of the i and i+3 positions.[15] In **19a**, $\phi(i)$ and $\psi(i)$ measure −49.2(4)° and 133.4(3)°, respectively, in good accordance with most of the other type I′ double β-turns examined in this study (Table S4.03). The same dihedrals measure 50.3(4)° and 46.3(4)°, respectively, in **19b**. Thus, there is a difference of 99.5° in $\phi(i)$ and 87.1° in $\psi(i)$ between the two structures, with **19b** exhibiting the only positive $\phi(i)$ value and the most acute $\psi(i)$ value in the entire data set. Perhaps coupled to the unusual main-chain dihedrals of **19b** is the *gauche* $\chi_1(i)$ value of −51.3(4)°. In **19a**, $\chi_1(i)$ measures −175.0(3)°, which is much more reflective of the remainder of the type I′ β-turn structures that tend to have *anti*-periplanar $\chi_1(i)$ values (Table S4.32). At the *C*-terminus of **19b**, $\phi(i+3)$ and $\psi(i+3)$ measure −117.8(4)° and −175.9(3)°, respectively, compared to −99.8(4)° and 41.4(4)° in **19a** (Table S4.03). These differences reflect the more extended backbone of **19b**. In this case, perceived deviations in the Leu side-chain orientation are almost entirely due to differences in the backbone, as the $\chi_1(i+3)$ values of **19a** and **19b** are approximately equal at −63.9(4)° and −64.4(4)°, respectively (Table S4.32).

DFT Optimization of the crystallographic coordinates provided energy minimized structures of **19a** and **19b** that overlay with the corresponding X-ray crystal structures with loop RMSDs of 0.13 and 0.06 Å, respectively (Figure 10). The optimized structure of **19a** has loop dihedrals that are much more similar to the canonical values than was observed in the solid state, hence the relatively high loop RMSD. Furthermore, the central β-turn H-bond shortens and becomes more directional, but the N−H(i+3)···O(i−1) β-turn H-bond breaks down completely upon geometry optimization. Instead, the *N*-terminal carbamate torques about $\phi(i)$ in such a way as to orient N−H(i) toward the opposite strand. The *C*-terminal ester, however, remains oriented away from the *N*-terminal strand, and a hairpin H-bond is not present. Only minor adjustments to the geometry of **19b** are observed after optimization, with an attendant lengthening of both β-turn H-bonds to values above 3.0 Å. An overlay of the two

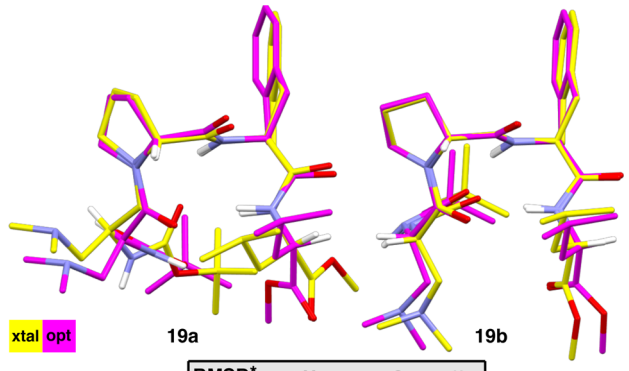

	RMSD* (Å)	ΔH (kcal/mol)	ΔG (kcal/mol)	μ (D)
19a	0.129	3.11	2.07	8.79
19b	0.061	0.00	0.00	9.85

*Loop region RMSD

Figure 10. Two solid-state conformations of peptide **19** were optimized using DFT at the M06-2X/6-311++G(2d,3p)//B3LYP/6-31+G(d,p) level of theory.

optimized geometries reveals that the primary deviation is in the *N*-terminal residue—the orientation of the backbone and Dmaa side-chain (Figure S6.05). These differences amount to 2.07 kcal/mol in free energy in favor of conformer **19b**, which benefits from two H-bonding interactions relative to one in **19a**.

Crystal Structure Library Analysis. Thus far, the discussion has primarily focused on the difference among discrete conformers of a given peptide. The degree of variation that we observed motivated an analysis of the peptide X-ray crystal structure library as a whole (Chart 1), in search of trends that might provide insight into (1) the effect of primary sequence modifications on secondary structure and (2) the source of differences between and within structural archetypes.[15] While crystal packing forces and systematic effects certainly influence the solid-state structures to some degree, the primary goal of this study has been to observe, document, and quantify the conformational space available to β-turn-containing tetrapeptides. In a way, deviations caused by packing forces may help us achieve this goal, as systematic effects are unlikely to give rise to a truly inaccessible geometry.[49] Furthermore, analysis of the structure library as a whole has shown that similar structures tend to deviate from the canonical turn-potentials in similar ways, allowing us to draw conclusions based on average values within of a given structural motif. It is useful to consider the possible sources of these differences, as they often provide insight into the steric and stereoelectronic effects that govern secondary structure. A summary of our findings is presented in Figure 11, and additional details can be found in the Supporting Information. These structural considerations may prove relevant to the design and study of future peptide-based catalysts.

Backbone Dihedrals. Inspired by the work of Ramachandran and co-workers,[50] we assessed the conformational space occupied by each residue of our peptides using ϕ,ψ dihedral plots (Figure 11a−d). It is instantly clear from these Ramachandran plots that the i+1 and i+2 residues are more tightly grouped than the i and i+3 residues. This is perhaps unsurprising given that the i+1 and i+2 residues comprise the loop-region of these peptides, which is biased to favor nucleation of a β-turn in every case by taking advantage of

DOI: 10.1021/jacs.6b11348
J. Am. Chem. Soc. 2017, 139, 492−516

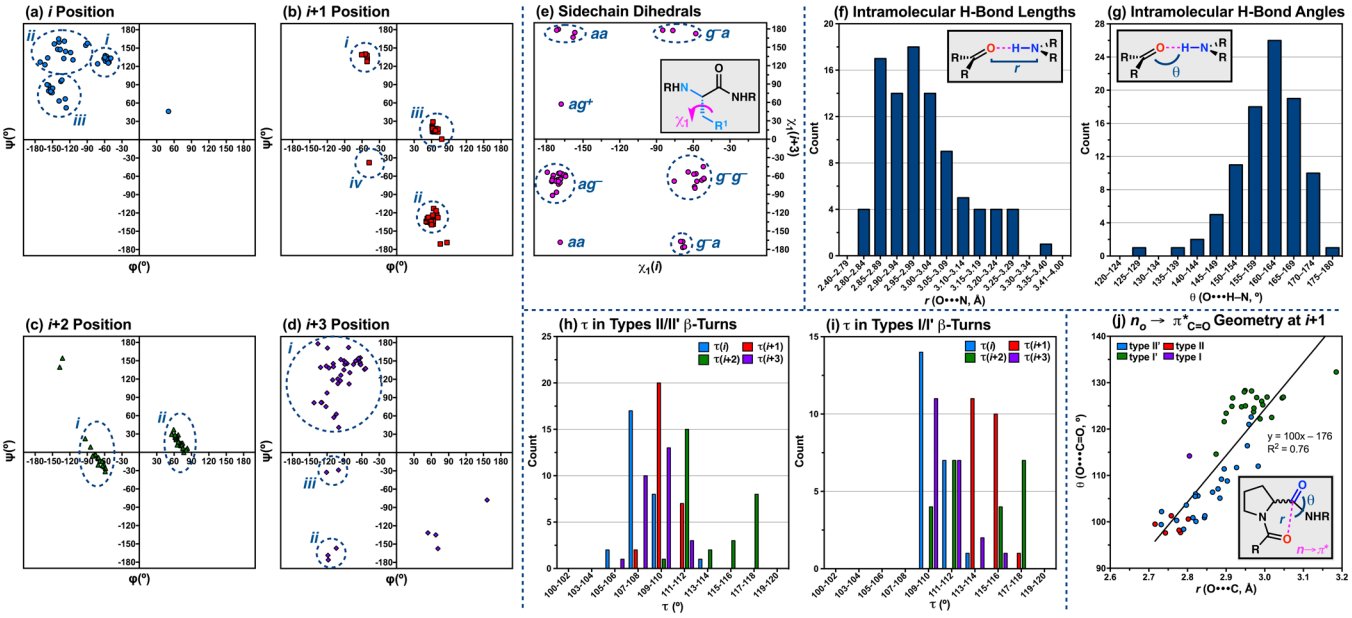

Figure 11. Structural attributes of the peptide X-ray crystal library. Ramachandran plots show the ϕ,ψ distribution at the (a) i, (b) i+1, (c) i+2, and (d) i+3 positions. Groupings of similar structural types are labeled in each plot. (e) A plot of $\chi_1(i+3)$ as a function of $\chi_1(i)$ shows the distribution of side-chain dihedrals. Histograms of H-bond (f) lengths and (g) angles show the distribution of H-bond geometries. Histograms of main-chain angles (τ) in (h) type II/II′ β-turns and (i) type I/I′ β-turns show the differences between the two secondary structural types. (j) A loose correlation between O(i)···C′(i+1) length and O(i)···C′=O(i+1) angle is observed for the $n \rightarrow \pi^*$ stereoelectronic interaction that stabilizes the turn.

the Pro-Xaa sequence. Though the loop residues tend to cluster more tightly than the peripheral residues, they still show a number of interesting deviations from the canonical values (Figure 2b).[3]

i+1 Position. The Ramachandran plot of the i+1 residue shows four relatively tight groupings corresponding to the four common β-turn motifs (i–iv, Figure 11b). Because the i+1 residue is either D- or L-Pro in all of the peptides analyzed, the clusters tend to center on ±60° in ϕ, the value set by the pyrrolidine ring.[3,21] The type II cluster (i, Figure 11b) consists of six peptides with average ϕ and ψ values of −53.4 ± 3.7° and 135.8 ± 4.7°, respectively (Table S4.02). Approximately equal and opposite values are observed for the type II′ cluster (ii, Figure 11b), with average ϕ = 60.6 ± 5.0° and average ψ = −130.2 ± 6.6° based on 23 peptides (Table S4.01). In both cases, the ψ value is noticeably wider than the ideal value of 120°, which may be related to repulsive interactions between the N−H(i+2) and N−H(i+3) σ-bonds, as discussed previously. The wider ψ value also permits a more geometrically favorable $n_{O(i)} \rightarrow \pi^*_{C'=O(i+1)}$ interaction, which is known to stabilize β-turns.[51] The type I′ cluster (iii, Figure 11b) consists of 21 peptides, significantly more than might have been expected from this library given the bias toward type II/II′ β-turns. It is perhaps noteworthy to mention that all of the type I′ β-turns observed in the solid state exist in the prehelical geometry described above by virtue of the N−H(i+2)···O(i−1) intramolecular H-bond. The average value of ϕ for this cluster is 65.3 ± 4.3°, and the average ψ value is 14° contracted relative to the ideal at 16.0 ± 5.1° (Table S4.03). These departures are consistent with an orientation of the loop amide that both promotes N−H(i+2)···O(i−1) H-bonding and minimizes $n_{O(i)}$-$n_{O(i+1)}$ Pauli repulsion. The lone type I β-turn (iv, Figure 11b) is peptide **37**, a structure we reported previously.[29c] The distorted type I β-turn is characterized by ϕ and ψ dihedrals measuring −47.7(3)° and −37.8(4)°, respectively. These values are perhaps buttressed by a 10-membered ring, side-chain-to-main-chain H-bond between N−H(i+2) and the free imidazole nitrogen-atom of the His(τ-Bn) side-chain, reminiscent of an ASX-turn.[52] The two outlying points centered around ϕ,ψ = 81°, −170° correspond to the symmetry-independent conformers of peptide **32** (**32a** and **32b**), both of which were largely unfolded in the solid state despite being biased toward a type II′ β-turn using a D-Pro-Phe central sequence (Figure S3.33). We also note parenthetically that we were able to rule out the Cγ-pucker of Pro as a relevant source of differences in the ϕ,ψ dihedrals of the peptides (Table S4.20–S4.24).[53]

i+2 Position. Unlike in the i+1 position, many different residues are found at the i+2 position in the structure library, ranging from Gly to a variety of α,α-disubstituted residues (Chart 1). Nevertheless, only two clusters are observed in the Ramachandran plot (Figure 11c), because ψ = 0° in all of the common turn-motifs, and the ideal ϕ values of types I/II′ (−90°/−80°) and types I′/II (90°/80°) are too proximal to distinguish them (Figure 2b).[3] The first cluster (i, Figure 11c) is composed of one type I and 23 type II′ β-turns. Again, the lone type I turn (**37**) is distorted in i+2 owing to its ASX-like turn geometry, with ϕ,ψ = −63.5(4)°, − 21.8(4)°. The average $\phi,\psi(i+2)$ values for the type II′ β-turns are −69.9 ± 9.1° in ϕ and −11.7 ± 12.0° in ψ (Table S4.01). Moreover, a wide span of ψ values were observed, ranging from −31.4° to 22.5°, and giving rise to a standard deviation greater than the mean. The ψ = 22.5(2)° data point corresponds to Ala-containing peptide **31** and might be an outlier of the cluster, the average of which lies below the negative ψ region. The second grouping (ii, Figure 11c) includes six type II and 21 type I′ β-turns. The average dihedrals for the type II β-turns measure 67.6 ± 8.3° in ϕ and 17.8 ± 12.6° in ψ (Table S4.02). The 28.7° range in ψ, as well as the large standard deviation of 12.6°, suggests that a variety of torsions are accessible within this archetype. The type I′ β-turns differ only slightly from the type II, with average ϕ and ψ of 69.1 ± 7.3° and 17.1 ± 9.3°, respectively (Table S4.03). In this case, wide ranges of 27.0° in ϕ and 33.0° ψ are observed. It

DOI: 10.1021/jacs.6b11348
J. Am. Chem. Soc. 2017, 139, 492–516

is perhaps noteworthy that, within each grouping, the Acpc-containing peptides tend to have values closer to $\psi = 0°$ than other $i+2$ variants. This may be related to the fact that Acpc tends to occupy the so-called "bridge region" of the Ramachandran plot, as highlighted by Toniolo and co-workers,[24a] owing in part to the wide main-chain angle that relieves the repulsive interaction between N−H($i+2$) and N−H($i+3$) to some degree.[43] The unfolded peptides **32a,b** are outliers ($\phi,\psi = -135°, -147°$) at this position, as well (Figure S3.33).

It is noteworthy that all four turn-types tend to deviate from their canonical $\phi,\psi(i+2)$ values in the same overall direction, although the degree varies from type to type (Figure 11c). On average, $\phi(i+2)$ is 10−27° more acute than anticipated, and $\psi(i+2)$ is 12−22° wider. The deviations in ϕ are coupled to the pitch of the loop amide; the established potentials require a relatively close distance between N−H($i+2$) and N−H($i+3$) in the type II/II′ β-turns and between O($i+2$) and O(i) in the type I/I′ turns, and contraction of the ϕ value may alleviate these strains to some degree. The average $\phi(i+2)$ among the type I′ turns is nearly two-times more contracted relative to the type II/II′ turns, a possible manifestation of the N−H($i+2$)···O($i-1$) H-bonds that stabilize the prehelical, double β-turn structures. In terms of $\psi(i+2)$, the canonical value of 0° requires the $i+2$ carbonyl to perfectly bisect the α-substituents (Figure 12a). The fact that $\psi(i+2)$ is universally wider than

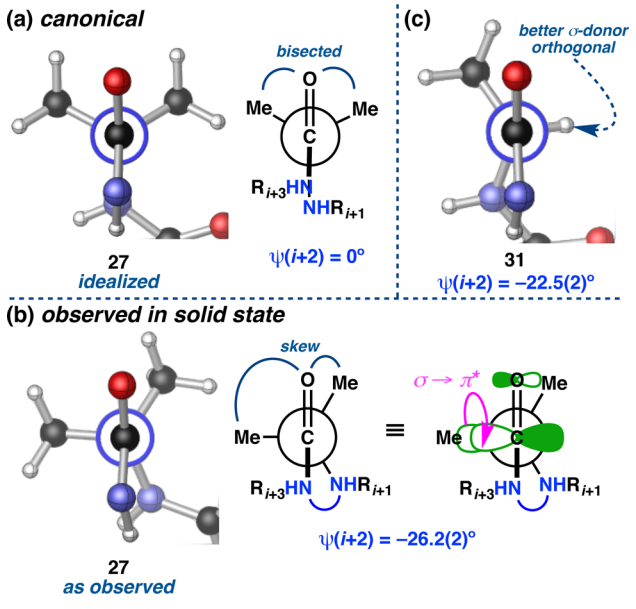

Figure 12. Deviations from canonical $\psi(i+2)$ values, as exemplified by peptides **27** and **31**. (a) The canonical value of $\psi(i+2)$ requires a bisected geometry. (b) In the solid state, however, a skew geometry is observed, which may be the result of an incipient $\sigma \rightarrow \pi^*$ stereoelectronic effect. (c) Ala-containing peptide **31** is skewed in the opposite direction relative to the other members of its type II′ β-turn class (e.g., **27**), possibly to achieve orthogonality between the C−H bond and the adjacent π-system.

typical suggests that a combination of steric and stereoelectronic factors may cause the $i+2$ α-substituents to torque either forward or backward, providing a skew conformation (Figure 12b,c). In the type I/II′ cluster, the α-substituents tend to pivot forward (toward the front/*endo* face of the β-turn) on average, while they tend to pivot backward (toward the back/*exo* face of the β-turn) in the type II/I′ cluster.

These observations appear consistent with an incipient $\sigma \rightarrow \pi^*$ stereoelectronic effect, wherein torquing about $\psi(i+2)$ orients one α-substituent orthogonal to the π-system of the $i+2$ carbonyl (Figure 12b). This hypothesis is supported by the following observations: (1) Acpc-containing peptides tend closer to the ideal $\psi(i+2)$ of 0°, as the sp^2 character of the cyclopropyl C−C bonds would make them poor σ-donors; and (2) Ala-containing peptide **31** is oriented such that its Cα−H bond, a better σ-donor than the C−Me bond, is orthogonal to the adjacent π-system, producing a ψ-deviation in the opposite direction of the other type II′ β-turns (Figure 12c). A stereoelectronic effect of this type would typically be associated with a shortening of the Cα−C′ bond. The lack of an appropriate zero-point has made this difficult to assess, but the directionality of the interaction, as governed by the relative orientation of the donor and acceptor, is favorable in each case. Both symmetry-independent molecules of Gly-containing peptide **33** are nearly ideal in $\phi(i+2)$ and $\psi(i+2)$, suggesting that a steric effect, such as allylic strain minimization about the loop amide, may be coupled to these stereoelectronic effects.

i Position. The ϕ,ψ plot for the i position is more diffuse than either of the two loop positions, but some grouping of similar structural types is observed nonetheless (Figure 11a). For example, most of the type I′ double β-turns tend to tightly cluster together due to the fact that the i position of these prehelical structures also serves as the first loop residue in the *N*-terminal, type II β-turn of the double turn-motif (*i*, Figure 11a). The ASX-turn-containing peptide **37** also appears in this cluster, but outside of the main grouping. The average $\phi(i)$ and $\psi(i)$ values of −56.3 ± 4.6° and 131.7 ± 3.5°, respectively, closely align with those measured for the type II cluster in the ϕ,ψ plot of the $i+1$ position (*i*, Figure 11b, Table S4.06). Deviations from the canonical type II potentials are likely due to the N−H($i+3$)···O(i) H-bond, which affects the *N*-terminal β-turn in much the same way as the N−H($i+2$)···O($i-1$) H-bond affects the central β-turn. The single outlier at ϕ,ψ = 50.3°, 46.3° corresponds to **19b**, which belongs in this cluster based on its overall topology but has quite different i dihedrals. All of the type II and II′ β-turns split into two relatively loose clusters based on the degree of backbone bending observed. Type II/II′ β-turns and hairpins with extended backbones are characterized by anticlinal ϕ and ψ values (*ii*, Figure 11a), with a mean ϕ of −133.8 ± 23.0° and a mean ψ of 145.9 ± 13.6° (Table S4.07). On the other hand, type II′ β-hairpins with bent backbones also have anticlinal ϕ values but are more *gauche* in ψ (*iii*, Figure 11a), with mean ϕ and ψ values of −146.0 ± 11.2° and 79.8 ± 12.4°, respectively (Table S4.08). These data show that the directionality of N−H(i), and thus the ability to engage in an intramolecular hairpin H-bond, is related to $\phi(i)$, while the degree of backbone bending relates to $\psi(i)$ (Table S4.13 and Figure S4.06).

i+3 Position. Within the crystal structure library, the $i+3$ position shows the most residue variation. Unsubstituted and alkyl-substituted residues, such as Gly, Leu, Nle, Val, and Chg, as well as benzylic residues, including Phe, D-Phe, 3-Pal, and 2-Thi, are found at the $i+3$ position. As such, it is not necessarily surprising that there is a lack of obvious trend in the $i+3$ Ramachandran plot (Figure 11d). Of the 50 peptides possessing $i+3$ residues, 41 (82%) possess negative values of $\phi(i+3)$ and positive values of $\psi(i+3)$ (*i*, Figure 11d), the averages being −93.7 ± 25.2° and 128.6 ± 32.1°, respectively

DOI: 10.1021/jacs.6b11348
J. Am. Chem. Soc. 2017, 139, 492−516

(Table S4.09). The large standard deviations reflect the diffuseness of the cluster, though there does seem to be some preference for orthogonal $\phi(i+3)$ and anticlinal $\psi(i+3)$. The three D-Phe-containing peptides (**14** and **21a,b**) are found in the bottom-right quadrant, as expected for an inversion of the α-stereocenter. Peptides **7a** and **7b** are also outliers at $i+3$ for reasons previously discussed. It is difficult to say whether or not the cluster centered on $\phi,\psi = -115°,-168°$ (*ii*, Figure 11d) is a group of outliers or a continuation of the main cluster (*i*, Figure 11d). Interestingly, the symmetry-independent conformers of peptide **33** are outliers (*iii*, Figure 11d). As discussed previously, the unusually acute (and negative) ψ-values orient the $i+3$ carbonyl away from the *N*-terminal strand, whereas the carbonyl typically points toward the opposite strand.

Side-Chain Dihedrals. Since the pioneering work of Dunbrack and co-workers,[15,54] the interplay of the side-chain dihedrals with those of the backbone, as well as their overall influence on protein structure, have become well appreciated. The steric and electronic profiles of side-chains have informed studies that aim to define "allowed" and "forbidden" χ-dihedral space for combinations of amino acids and to apply these parameters in a predictive manner.[55] In an effort to contribute to this growing literature, we analyzed the χ_1 dihedrals at the i and $i+3$ positions of our peptide crystal structure library and plotted $\chi_1(i+3)$ against $\chi_1(i)$ in search of structural trends (Figure 11e). To avoid ambiguity, Val-containing peptides **9**, **10**, and **26** and Chg-containing peptide **11** were removed from this analysis, as were the peptides without $i+3$ residues or side-chains (**7a,b** and **35**−**37**).

Perhaps the most obvious characteristic of this plot is that no positive χ_1 values were observed at the i position (Table S4.32). Negative $\chi_1(i)$ values orient the side-chain away from the peptide scaffold so as to minimize unfavorable steric interactions. Positive values of $\chi_1(i+3)$ are relatively uncommon for similar reasons, with over 82% of the peptides analyzed having negative $\chi_1(i+3)$ values. Moreover, the side-chains at both the i and $i+3$ positions tend to cluster around *gauche* (g) and *anti* (a) values of χ_1, the expected minima on the torsional potential energy surface of amino acid−based systems (Tables S4.33−S4.37). About 75% of the peptides are *gauche* at the $i+3$ position, while the i position is more evenly split between *gauche* and *anti* (40:60). The two major clusters are ag^- (i.e., *anti* at *i*, negative *gauche* at $i+3$), consisting of 21 peptides, and g^-g^-, comprising 11. The type I′ double β-turn structures demonstrate a strong preference for the ag^- arrangement of side-chains, as 17 out of the 19 such peptides analyzed are found in the ag^- cluster. Further, all but one of the type I′ peptides have *anti* $\chi_1(i)$ values, and all of them have *gauche* $\chi_1(i+3)$ values (Table S4.38). The only type I′ peptide to have a *gauche* $\chi_1(i)$ is **19b**, and the lone ag^+ peptide is **4e**, also a prehelical, type I′ β-turn, both of which were discussed previously. It is plausible that *anti* $\chi_1(i)$ values are favored because they orient the side-chain as far away as possible from both the backbone and the *C*-terminal side-chain. It seems that the preference for *gauche* $\chi_1(i+3)$ values avoids destabilizing *syn*-pentane-type strain with the *C*-terminus, while also promoting a more compact structure. The side-chains of the type II/II′ β-turns are significantly less directional and appear in all of the clusters. Of the 23 examined, about 35% have *anti* $\chi_1(i)$ values, and 61% have *gauche* values of $\chi_1(i+3)$ (Table S4.38). This suggests that *gauche*/*anti* differential is less energetically significant at both the i and $i+3$ positions among the type II/II′ β-turns.

H-Bond Geometries. The ability to form intra- and intermolecular H-bonds is a fundamental feature of peptides that is essential to their higher order structures and functions. In the context of β-turns, intramolecular H-bonds stabilize the folded structure, and intermolecular H-bonds play a role in association with molecular guests or other peptides.[14,20] The H-bonding patterns of our peptide X-ray crystal structure library were analyzed and compared with known data. Only amide−amide H-bonds are considered in our analysis to ensure a proper reference point. We found the H-bonding patterns of our crystal structures to be typical overall.[56]

The N···O distances (r) and N−H···O angles (θ) for 94 intramolecular, amide−amide H-bonds were measured and analyzed. Four different types of intramolecular H-bonds are observed across our library: (1) N−H($i+3$)···O(i) β-turn H-bonds found in every member of the library except unfolded peptides **32a** and **32b**, (2) N−H(i)···O($i+3$) hairpin H-bonds found in types II′ and II β-turns, (3) N−H($i+2$)···O($i-1$) β-turn H-bonds found exclusively in the type I′ double β-turns, and (4) N−H($i+2$)···O(i) γ-turn H-bonds observed sporadically. While the distances were often favorable for γ-turn H-bonding, the angles were often too acute to be relevant, and thus we excluded the N−H($i+2$)···O(i) metrics from this analysis. There are only minor differences among the other three types of H-bonds. The average value of r across the whole set measures 3.005 ± 0.124 Å, with a median of 2.979 Å. A range of 2.804−3.358 Å was observed, spanning from strong to very weak intramolecular H-bonds.[56] A histogram showing the distribution of r values possesses two local maxima, one at 2.85−2.89 Å and the other at 2.95−2.99 (Figure 11f). Another interesting feature of the distribution is the relatively high proportion of H-bonds with r greater than 3.20 Å. Above this length, H-bonds tend to be quite weak. It may even be tempting to discount these interactions as proper H-bonds. However, we included them in the analysis if the N−H···O angles were appropriately directional. The average value of θ measures 160 ± 8°, which is typical for amide−amide H-bonds in the solid state. A range of 127° to 175° was observed, and the distribution is skewed toward the higher end of the range (Figure 11g). The most favorable H-bonds have a near linear N−H···O angle, but this is difficult to achieve given the geometric constraints of the β-turn structure. The values at the lower end of this distribution may be questionable as to whether they constitute a true H-bond or not, but they were included on the basis of their lengths.

Main-Chain Angles. The ideal value of a main-chain angle (τ) can be considered to be 109.5°, in accord with a perfectly tetrahedral α-carbon.[15] It is not uncommon, however, to observe a range of τ values, especially for those residues involved in secondary structures.[43] The main-chain angles of each residue in our peptide library were measured, providing 208 τ values for analysis. We observe a distribution of τ values ranging from 105.9° to 118.1°, with a mean of 111.5 ± 2.8° and a median of 110.8° (Table S4.25). The average τ is likely skewed larger than tetrahedral due to the prevalence of Acpc residues in our library, which have wide τ values on average (117.2 ± 0.6°). A τ histogram shows a clear maximum at tetrahedral values (109−110°) and perhaps more wide-angle counts than might be expected (Figure S4.08). When analyzed on a position-by-position basis, some interesting trends are observed (Figure S4.09). The peripheral residues tend to be tetrahedral on average, with averages for $\tau(i)$ and $\tau(i+3)$ measuring 109.5 ± 1.7° and 110.3 ± 1.7°, respectively.

DOI: 10.1021/jacs.6b11348
J. Am. Chem. Soc. 2017, 139, 492−516

However, the loop-region angles are significantly wider. The mean $\tau(i+2)$ measures 113.9 ± 2.9°, which is perhaps skewed wide due to the 20 peptides that have an Acpc residue at the $i+2$ position. As such, the $\tau(i+2)$ histogram is bimodal, with maxima at 111−112° and 117−118° (Figure S4.08). Though all of the peptides possess a D- or L-Pro residue at the $i+1$ position, the average value of $\tau(i+1)$ is also quite wide at 112.2 ± 2.5°.[57] As there are no strained rings at $i+1$, this widening must be a result of the conformational stresses imposed by the well-defined β-turn loop-region. The $\tau(i+1)$ histogram also shows two maxima, one at 109−110° and the other at 113−114°; there is a comparatively large proportion of $\tau(i+1)$ values in the 115−116° range, as well.

Analyzing the τ positional distributions as a function of turn-motif provided some additional insight. In the type II/II′ β-turns, the $\tau(i+1)$ distribution is centered at approximately tetrahedral (Figure 11h), with a mean value of 110.1 ± 1.0° (Table S4.27). Among the type I/I′ β-turns, however, $\tau(i+1)$ averages 114.9 ± 1.0°, nearly equal to the 114.2 ± 2.9° mean $\tau(i+2)$ value (Table S4.29). The distribution is skewed quite wide, as well; no $\tau(i+1)$ values are found below 113−114°, which is also the bin with the highest count (Figure 11i). These data suggest that the observed widening of $\tau(i+1)$ across the whole library is due to the presence of the 22 type I/I′ β-turns, which have significantly wider $\tau(i+1)$ values on average than their type II/II′ counterparts. In fact, the entire distribution is shifted wide compared to that of the type II/II′ turns, including the peripheral positions. From a conformational standpoint, we attribute this widening to the prehelical geometry of the type I/I′ β-turns. This is especially evident at the $i+1$ position, wherein the proximal and codirectional i and $i+1$ carbonyls may induce n_O−n_O Pauli repulsion that widens $\tau(i+1)$ angle (Figure 13a).[58] This proposed interaction is absent in the type II/II′ β-turn structures, in which the carbonyls are oriented in opposite directions.

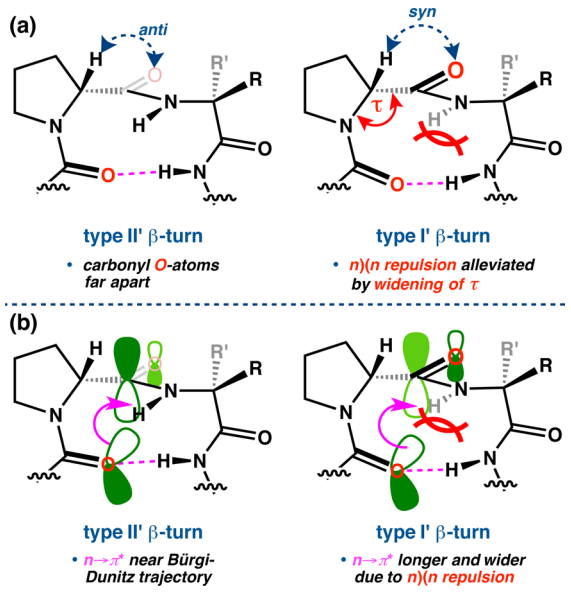

Figure 13. Some differences between type II′ and I′ β-turns. (a) Widening of $\tau(i+1)$ as a consequence of Pauli repulsion in type I′ β-turns. (b) As a consequence of this repulsion in type I/I′ turns, types II/II′ are able to access a more favorable $n \rightarrow \pi^*$ geometry, with shorter interaction O···C′ distances and near Bürgi−Dunitz trajectories.

$n \rightarrow \pi^*$ Geometries. We also examined the peptide library for its exhibition of the $n \rightarrow \pi^*$ stereoelectronic effect, wherein lone pair electron density localized on the carbonyl oxygen-atom of the i residue donates into the antibonding π-orbital of the proceeding $i+1$ carbonyl.[51,58,59] This type of delocalization stabilizes the β-turn via a partial bonding interaction that tethers O(i) to C′($i+1$). The most favorable $n \rightarrow \pi^*$ interactions are typically shorter than the sum of the van der Waals radii of the two atoms (r < 3.2 Å) and have O···C═O angles (θ) near the Bürgi-Dunitz trajectory (θ = 107−110°).[60] In order to assess the degree to which $n \rightarrow \pi^*$ effects are present in this structure library, we measured the O(i)···C′($i+1$) lengths and O(i)···C═O($i+1$) angles for each peptide.

The average O(i)···C′($i+1$) distance measures 2.893 ± 0.098 Å, with a range from 2.716 to 3.185 Å (Table S4.44), consistent with the operation of $n \rightarrow \pi^*$ effects. However, the average O(i)···C′═O($i+1$) angle is wider than the Bürgi-Dunitz trajectory at θ = 113.6 ± 11.3°. Plotting θ against r reveals a loose correlation between length and angle (R^2 = 0.76) with a positive slope; longer distances tend to accommodate wider angles and *vice versa* (Figure 11j). These $n \rightarrow \pi^*$ effects are thus perturbed by additional local structural contexts.

When analyzed as a function of β-turn motif, the data again show differences between the canonical turn-types. The six type II β-turns are characterized by average r and θ values of 2.763 ± 0.031 Å and 99.2 ± 1.6°, respectively, the shortest and most acute $n \rightarrow \pi^*$ geometries observed for the set (Table S4.45), whereas the average of the 23 type II′ β-turns measures 2.857 ± 0.071 Å in r and 106.8 ± 6.7° in θ (Table S4.46). The more favorable interaction geometries in the type II turns may be coupled to their $\phi,\psi(i+1)$ dihedrals, which are more distorted on average relative to the diastereomeric type II′ turns (*i* vs *ii*, Figure 11b). The widening of $\psi(i+1)$, especially, accommodates a more acute O(i)···C′═O($i+1$) angle, and therefore allows for a shorter O(i)···C′($i+1$) distance. However, the 21 type I′ double β-turns exhibited longer O(i)···C′($i+1$) distances and wider O(i)···C′═O($i+1$) angles, with an average r and θ values of 2.974 ± 0.067 Å and 125.2 ± 3.5°, respectively (Table S4.47). It is possible that this may be coupled to the wider $\tau(i+1)$ observed for this turn-motif, as the structures must balance the effects of destabilizing n_O-n_O Pauli repulsion, N−H($i+2$)··· O($i-1$) H-bonding, and favorable $n \rightarrow \pi^*$ overlap (Figure 13b).[58] Thus, the $n \rightarrow \pi^*$ geometries may tend toward a less favorable donor−acceptor orientation to maximize the O(i)··· O($i+1$) distance. Though it has been shown that the Cγ-pucker of Pro can affect $n \rightarrow \pi^*$ geometry in model systems,[51] this issue is not obviously a source of deviation among the β-turn-types in this library.

Stereoelectronic effects of this type might be expected to produce concomitant lengthening of C═O($i+1$) and pyramidalization of C′($i+1$). Possibly due to the lack of a proper zero-point, we were unable to observe any significant lengthening of C═O($i+1$); the average length across the entire library measures 1.228 ± 0.006 Å, which is identical to the often quoted value of 1.23 Å. However, the pyramidalization of C′($i+1$), as measured by $\Delta_{C'}$, is non-negligible, with a mean $\Delta_{C'}$ of 0.10 ± 0.08 Å (Table S4.44).[44] The large standard deviation reflects significant variation within the data set. Interestingly, the type I′ β-turns show the most significant pyramidalization of C′($i+1$) despite their nonideal interaction geometry (average $\Delta_{C'}$ = 0.014 ± 0.007 Å). This is likely a function of the inherent strains in this turn-motif.

DOI: 10.1021/jacs.6b11348
J. Am. Chem. Soc. 2017, 139, 492−516

Distribution of Turn-Types and Homologous Structure Series. We now discuss structural data for three series of homologous peptides, including those that vary only at the *i*+2 position, those that differ at the *C*-terminal cap, and those containing L-Pro instead of D-Pro. These data enable a systematic comparison of structures that differ by a single substitution. Discussion of the relationship between peptide structure and catalytic activity in the bromination of quinazolinone **1**, namely enantioselectivity, are discussed where appropriate.[61]

Effects of the i+2 Residue. The *i*+2 residue plays an important role in the nucleation and conformational stabilization of a β-turn.[3,11] We intentionally biased all of the peptides in this structure library to adopt either type II′ or type II β-turns depending on whether D- or L-Pro was incorporated at the *i*+1 position. However, we observed a wider range of turn-motifs in the solid state than initially expected, and we wondered how the nature of the *i*+2 residue might influence this distribution. Figure 14 presents the incidence of canonical β-turn-types as a function of *i*+2 residue.[62]

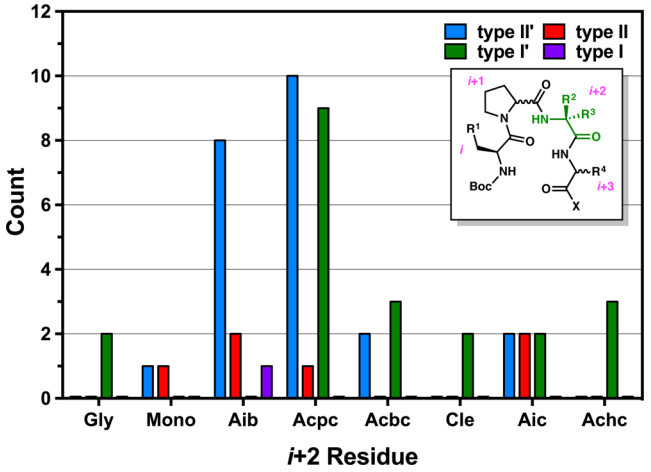

Figure 14. Occurrence of canonical turn-motifs as a function of *i*+2 residue. Peptide **32** was excluded from this analysis.

Over half of the library (nearly 57%) consists of Aib- and Acpc-containing peptides, and the data show a significant difference between these two subsets. While the Aib-containing peptides largely tend to nucleate the anticipated type II/II′ turns depending on the Pro stereochemistry, those with Acpc residues at the *i*+2 are more bimodal—that is, they are distributed more evenly among the type II/II′ and prehelical, type I′ turns. The lone type I turn (peptide **37**) contains a central L-Pro-Aib sequence, which suggests circumstantially that the type I′ conformation should also be accessible for Aib-containing peptides. Even so, none were observed in this library. Despite the fact that Aib and Acpc only differ by an equivalent of molecular hydrogen, they seem to behave differently in the context of β-turn structure. These data suggest that Acpc may allow for more conformational freedom than Aib in these particular sequences, possibly as a consequence of the strained cyclopropyl ring that widens $\tau(i+2)$ and allows access to the bridge-region of Ramachandran space.[63] The Acbc-containing peptides are also more evenly divided between types II′ and I′ turns, perhaps for similar reasons. It is interesting to note that the seemingly "Aib-like" residues, such as Cle, Aic, and Achc,[24] behave differently than Aib itself and are observed to promote the nucleation of prehelical type I′ β-turns in this context (Figure 14).

Crystallographic Analysis of Homologous i+2 Series. We were able to obtain X-ray crystallographic data for a homologous series of seven peptides that differ from one another only at the *i*+2 residue (Figure 15a). All of the peptides possess a common Boc-Dmaa-D-Pro-Xaa-Leu-OMe sequence that was designed to nucleate a type II′ β-hairpin. Of the seven homologues, only the Aib-containing peptide **25** exhibits the targeted secondary structure. All of the others (**4**, **17**−**19**, **22**, and **33**) present prehelical, type I′ β-turn structures in the solid state. An overlay of these six structures shows a tight correspondence in the loop-region (RMSD $\leq$ 0.11 Å) with more variability at the peripheral positions (Figure 15b). The *N*-terminal residues are more cohesive than those of the *C*-terminus. The Gly-containing peptide **33** is particularly noteworthy for its prehelical structure, as Pro-Gly sequences were previously studied as archetypal β-hairpin inducers.[19,22] The average value of $\tau(i+2)$ in **33** measures 115.5 ± 0.1° for the two symmetry-independent molecules **33a** and **33b**. Notably, the wide $\tau(i+2)$ observed for Gly is reminiscent of Acpc, and perhaps this signifies that Gly is similar to Acpc in terms of its influence over the conformational space available to β-turn-biased structures.

NMR Analysis of Homologous i+2 Series. To investigate whether or not the secondary structures observed in the solid state were populated in solution, we acquired NMR data for each member of the *i*+2 homologous series under identical conditions (600 MHz, 0.01 M, C_6D_6, 20 °C). The same protocol that was applied to peptide **4** (*vide supra*) was also used to analyze peptides **17**−**19**, **22**, **25**, and **33**. Additional details, including stacked ^{1}H NMR spectra (Figure S5.16), are provided in the Supporting Information. In general, as with compounds discussed earlier, our data are consistent with a variety of populated states for these peptides in solution.

The NMR data for Acbc-containing peptide **17** are quite similar to those of **4**. The $^3J_{NH-H\alpha}$ values extracted from the ^{1}H NMR spectrum are consistent with a $\phi(i)$ of approximately −30° and $\phi(i+3)$ values of either −89° or −151° (Table S5.40). As for **4**, these torsions can accommodate a variety of conformations, but they are perhaps most consistent with the prehelical and nonhairpin β-turns. The chemical shifts of the N*H*(Leu) and N*H*(Acbc) resonances suggest that these amides are involved in intramolecular bonds, while that of N*H*(Dmaa) is in-line with a non-H-bonded state (Table S5.41). It is notable that the N*H*(Leu) signal of **17** is 0.58 ppm more upfield than that of **4**; in fact it is the most upfield-shifted N*H*(Leu) signal of the entire homologous series (Figure S5.16), which intimates that the N*H*(*i*+3)···O(*i*) β-turn H-bond could be particularly weak in the case of **17**. Moreover, the following structure-suggestive NOE contacts are observed in the NOESY spectrum: Boc(Dmaa) ↔ N*H*(Acbc), Boc(Dmaa) ↔ N*H*(Leu), and δ(D-Pro) ↔ N*H*(Acbc). Although these correlations are supportive of a prehelical, type I′ β-turn structure, the presence of a moderate strength α(D-Pro) ↔ N*H*(Acbc) NOE indicates that **17** may sample type II′ loop dihedrals in solution (Figure S5.06). As such, these data support either a γ'-turn conformation similar to that proposed for homologue **16** or a prehelical structure mirroring the solid-state observations (**17a**,**b**) for this sequence.

Data gleaned from the NMR spectra of Cle-containing peptide **18** indicate that its most populated conformer in the solution phase differs from the type I′ double β-turn it shows in

DOI: 10.1021/jacs.6b11348
J. Am. Chem. Soc. 2017, 139, 492−516

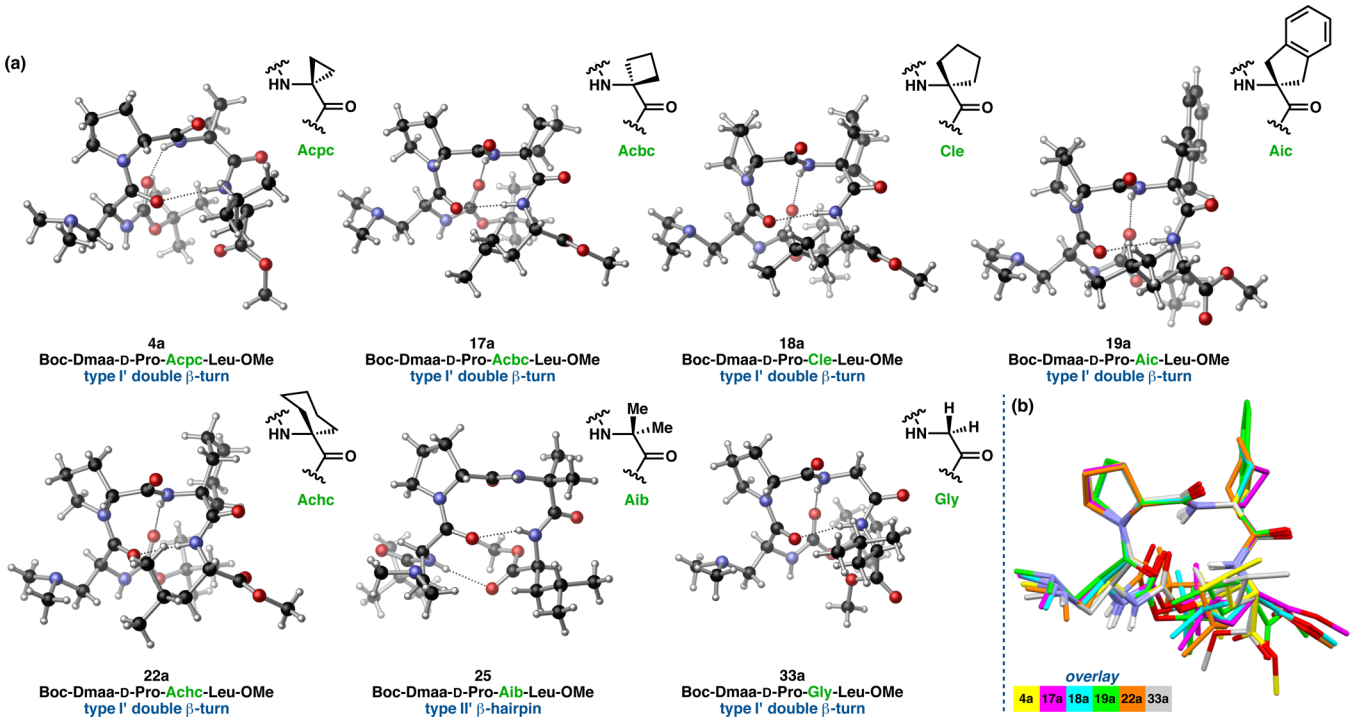

Figure 15. (a) Homologous series of peptides differing from one another only in the *i*+2 residue. For sequences with more than one symmetry-independent structure, only one is shown. (b) Overlay of the type I′ β-turns from the homologous series showing tight overlap in the loop-region and more deviations at the peripheral residues. All loop RMSDs are less than 0.11 Å. For more structural information, see Figure S4.21.

the solid state (**18a**,**b**). The $\phi(i)$ and $\phi(i+3)$ dihedral angles of **18** are calculated to be −63° or −177° and −89° or −142°, respectively, using the corresponding $^{3}J_{\mathrm{NH-H}\alpha}$ values (Table S5.40). These dihedrals are most in-line with those expected for a β-turn or hairpin. The relative chemical shifts of the amide resonances suggest that N*H*(Leu) is likely engaged in an N*H*(*i*+3)···O(*i*) H-bond, while N*H*(Cle) is largely solvent-accessible (Table S5.41). Compared to those of peptides **4** and **17**, the N*H*(Dmaa) signal of **18** occurs at a downfield shift and is significantly sharper in terms of peak width (Table S5.43). These chemical shift data are in-line with a hairpin conformation. Moreover, a number of long- and short-range NOE correlations are apparent in the NOESY spectrum of **18** (Figure S5.07), including the following structure-suggestive contacts: N*H*(Leu) ↔ N*H*(Cle), β(Dmaa) ↔ N*H*(Leu), δ(D-Pro) ↔ N*H*(Cle), and Boc(Dmaa) ↔ N*H*(Leu). A strong α(D-Pro) ↔ N*H*(Cle) NOE is also observed, providing evidence in support of type II′ loop dihedrals despite the NOE-contacts (e.g., the latter two) that point to a prehelical, type I′ structure. Overall, these NMR data are consistent with a type II′ β-hairpin solution structure that may also be in equilibrium with nonhairpin conformational states.

The solution structure of Aic-containing peptide **19** presents an intermediate case. The $^{3}J_{\mathrm{NH-H}\alpha}$ value of the *i* position is consistent with $\phi(i)$ dihedrals of either −89° or −142°, and that of the *i*+3 position yields $\phi(i+3)$ values of either −89° or −151° (Table S5.40). These calculated torsions are most representative of the β-turn and hairpin conformations, though the prehelical form cannot be rigorously excluded. The ^{1}H NMR chemical shifts for the N*H*(Leu) and N*H*(Dmaa) signals indicate that both are engaged in intramolecular H-bonds. The N*H*(Aic) resonance is less diagnostic; it is moderately downfield-shifted, which might suggest that it samples H-bonded and solvent-exposed states on the NMR time-scale (Table S5.41), although it could also be attributed to deshielding anisotropic effects stemming from the indane ring. A strong α(D-Pro) ↔ N*H*(Aic) correlation observed in the NOESY spectrum of **19** is consistent with a type II′ loop-region (Figure S5.08). Additional long- and short-range NOEs are also apparent, including fairly strong N*H*(Leu) ↔ N*H*(Aic) and N*Me*$_2$(Dmaa) ↔ δ(Leu) contacts, as well as weak δ(Leu) ↔ α(D-Pro), Boc(Dmaa) ↔ N*H*(Leu), and Boc(Dmaa) ↔ β(Aic) correlations. In the solid state, peptide **19** was found to exhibit distorted, prehelical, type I′ β-turn structures in both symmetry-independent conformers (Figure 9). In contrast, these NMR data suggest that **19** likely populates both type II′ β-hairpin and γ'-turn forms.

Peptides **22** and **25**, which contain Achc and Aib residues at the *i*+2 position, respectively, provided similar NMR data profiles. In both cases, the $^{3}J_{\mathrm{NH-H}\alpha}$ of the *i* position gives rise to calculated $\phi(i)$ values of either −67° or −172° (Table S5.40). The calculated $\phi(i+3)$ values differ only slightly between **22** and **25**, with those of the former being either −90° or −150° and those of the latter being −94° or −151°. These dihedrals are able to accommodate all of the proposed conformations. The ^{1}H NMR spectra of both peptides show downfield-shifted N*H*(Leu) and N*H*(Dmaa) resonances and particularly upfield-shifted N*H*(*i*+2) signals. These chemical shift data support conformations wherein N*H*(Leu) and N*H*(Dmaa) are engaged in intramolecular H-bonds, perhaps N*H*(*i*+3)···O(*i*) and N*H*(*i*)···O(*i*+3) H-bonds, while N*H*(*i*+2) is free (Table S5.41). The NOESY spectra of peptides **22** and **25** peptide differ slightly. Peptide **22** exhibits multiple long-range contacts that imply interstrand proximity (Figure S5.10). For example, the following NOEs are observed: Boc(Dmaa) ↔ β(Achc), α(Dmaa) ↔ N*H*(Leu), δ(Leu) ↔ γ(D-Pro), and a fairly strong α(D-Pro) ↔ N*H*(Achc) suggestive of type II′ loop dihedrals. Peptide **25** shares many of the short-range contacts exhibited

DOI: 10.1021/jacs.6b11348
J. Am. Chem. Soc. 2017, 139, 492−516

by **22** (Figure S5.11). Strong α(D-Pro) ↔ N*H*(Aib) and N*H*(Leu) ↔ N*H*(Aib) are consistent with type II′ loop dihedrals, but the absence of long-range NOEs might reflect a conformationally dynamic solution structure. Taken together, the data for peptides **22** and **25** are well aligned with type II′ β-hairpin conformations in solution, although it is important to acknowledge the possibility that nonhairpin conformations, such as a γ'-turn, may also be populated. This assignment is in agreement with the crystal structure of **25**, but for **22** the solution phase and solid-state structures point to different conformations, as its crystal structure presents a prehelical, type I′ conformation (Figure 15).

The solution NMR data of Gly-containing peptide **33** accommodate multiple conformational states. The $^3J_{NH-H\alpha}$ values of the peripheral residues are consistent with $\phi(i)$ dihedrals of either −119° or −180° and $\phi(i+3)$ dihedrals of either −89° or −151° (Table S5.40). These calculated torsions are most representative of the β-turn and hairpin conformations. The ^{1}H NMR resonances of N*H*(Leu), N*H*(Gly), and N*H*(Dmaa) occur at relatively downfield frequencies, suggesting that all three are involved in, or at least sampling, intramolecular H-bonds (Table S5.41). The longer-range NOE contacts observed in the NOESY spectrum of **33** provide evidence for interstrand proximity, but are not hallmarks of any specific conformation (Figure S5.14). These contacts are as follows: α(Dmaa) ↔ δ(Leu), γ(D-Pro) ↔ N*H*(Leu), γ(D-Pro) ↔ N*H*(Gly), and N*Me*$_2$(Dmaa) ↔ N*H*(Leu). Furthermore, a moderate-weak α(D-Pro) ↔ N*H*(Acbc) correlation perhaps demonstrate that type II′ turn dihedrals are favored to a lesser extent. This might be coupled to the weak N*H*(Leu) ↔ N*H*(Gly) NOE, which implies that a β-turn may not be the most populated state in solution. Overall, these data could signal a type II′ β-hairpin/γ'-turn equilibrium favoring the γ'-form. In the solid state, peptide **33** adopts a prehelical geometry in both symmetry-independent molecules (Figure 15). As these data do not necessarily preclude this conformation, it is possible that the prehelical form is also populated to some degree in solution.

It is interesting to note that, while six of the seven peptides in the homologous *i*+2 series can exhibit the prehelical, type I′ β-turn structure in the solid state (Figure 15), only one peptide definitively populates this conformation in solution (i.e., **4**). The solution NMR data presented above capture the dynamic behavior of these β-turn biased sequences in conditions relevant to catalysis.

Connections to Enantioselective Catalysis in the Homologous i+2 Series. Table 2 summarizes the observed solid-state and solution-phase conformations of the homologous *i*+2 peptides and presents the enantioselectivity exhibited in the bromination of quinazolinone **1** under the conditions of eq 2.

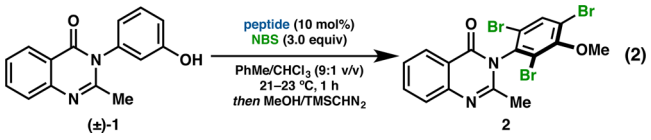

These data highlight the importance of the *i*+2 position in enantioselective catalysis, as the er of tribromide **2** ranges from 61:39 to 95:5 depending on the identity of this residue. We note that conversion is complete in every case. Interestingly, the enantioselectivity decreases as a function of ring size in the nominally spirocyclic *i*+2 residues, with strained rings (e.g., Acpc and Acbc) providing higher selectivities. The only exception is Aic-containing **19**, which is the least selective catalyst and provides **2** in only 61:39 er. Although Aic is related to Cle, the benzo-ring of Aic could either (a) induce conformational changes in the catalyst structure that render it less selective or (b) interact with the substrate via π-stacking interactions that are deleterious to enantioinduction. Moreover, Achc-containing **22** performs comparably to Aib-containing **25**, which might be expected given that they both adopt type II′ β-hairpins in solution. What is surprising, however, is the low er of 68:32 observed for both **22** and **25**, as our hypothesized model for enantioinduction invokes docking of **1** to a type II′ β-hairpin conformer of peptide **3**.[28a] Indeed, the best catalysts for this reaction are found to adopt nonhairpin conformations in the solid state and in solution. Acpc-containing peptide **4** significantly outperforms **3**, yet it adopts a prehelical, type I′ β-turn in its crystal and NMR structures. Additionally, Gly-containing **33** is nearly as selective as **3**, delivering **2** in 91:9 er despite the lack of α-substituents at the *i*+2. Catalyst **33** was also found to adopt a prehelical, type I′ β-turn in the solid state, and it is most likely in fast-exchange equilibrium between multiple conformers in solution.

Table 2. Enantioselectivity Observed for Homologous *i*+2 Series[a]

	i+2 Residue	Solid-State Conformation[b]	Solution Conformation[c]	Average er[d]
4	Acpc	pre-helical type I' β-turn*	pre-helical type I' β-turn	95:5
17	Acbc	pre-helical type I' β-turn*	γ'-turn/pre-helical type I' β-turn	83:17
18	Cle	pre-helical type I' β-turn*	type II' β-turn	70:30
19	Aic	pre-helical type I' β-turn*	type II' β-hairpin/ γ'-turn	61:39
22	Achc	pre-helical type I' β-turn*	type II' β-hairpin	68:32
25	Aib	type II' β-hairpin	type II' β-hairpin	68:32
33	Gly	pre-helical type I' β-turn*	γ'-turn/type II' β-hairpin	91:9

[a] Reaction Conditions: **1** (0.05 mmol, 1 equiv), peptide (0.005 mmol, 10 mol%), NBS (0.15 mmol, 3 equiv w.r.t. **1**), PhMe/$CHCl_3$ (9:1 v/v, 0.01 M w.r.t. **1**), 21–23 °C (NBS added in one portion). [b] Observed solid-state confromation. An asterisk (*) denotes that this conformation was exhibited in multiple, distinct states (i.e., symmetry-independent conformers or polymorphs). [c] Observed solution-phase NMR structure (0.01 M, C_6D_6, 20 °C). In cases where more than one option is listed, NMR data is consistent with more than one conformation. [d] Measured er of tribromide **2** determined by chiral HPLC. Average of two trials.

Taken together, these results suggest that peptidic catalysts that nucleate rigid β-turns are not necessarily the most effective in the context of this atroposelective bromination reaction. In fact, there seems to be some benefit to catalyst flexibility that is not yet fully understood. There are a number of caveats associated with making enantioselectivity predictions based on structurally dynamic catalysts.[33] In this particular reaction, however, both highly strained (e.g., Acpc) and unstrained (e.g., Gly) *i*+2 residues provide highly selective catalysts. This unusual dichotomy suggests that more global conformational effects are likely operative along the selective reaction coordinate.

Role of Peripheral Residues. While the peptide library analyzed in this study is highly populated with sequences containing a Dmaa residue at the *i*-position, peptides with other

DOI: 10.1021/jacs.6b11348
J. Am. Chem. Soc. 2017, 139, 492–516

residues in this position show similar properties. For example, the ability to access a type I′ double β-turn geometry does not seem to require a Dmaa residue at the *i* position. Peptide **5**, a homologue of peptide **4** in which the Dmaa residue has been substituted with Cys(Ph), also adopts the prehelical geometry (Figure 16a). The same is true of peptide **23**, the Cys(Ph)

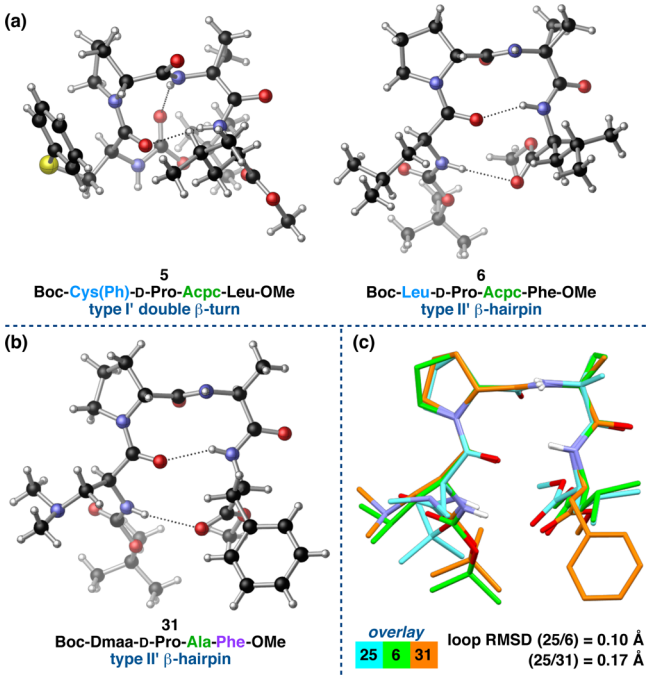

Figure 16. (a) Two *i* position homologues of peptide **4**, Cys(Ph)-containing **5** and Leu-containing **6**. (b) The Ala-containing peptide **31** is not quite homologous to the series presented in Figure 15 due to its *i*+3 Phe residue. (c) An overlay shows the structural similarity between type II′ β-hairpins **25**, **6**, and **31**.

variant of **22** (Figure S3.24). However, peptide **6**, the carbon-isostere of **4** in which the *i* residue is Leu instead of Dmaa, adopts a typical type II′ β-hairpin geometry (Figure 16a). We do not expect that this difference is due to the Leu residue specifically, but rather it reflects the bimodal distribution of Acpc-containing peptides.

The Ala-containing peptide **31** is not a perfect structural homologue of **6** owing to the *i*+3 Phe residue, but its type II′ β-hairpin structure closely resembles that of **6** (Figure 16b). Additionally, the structures of both **6** and **31** are quite coincident with Aib-containing peptide **25**, with loop RMSDs of 0.10 and 0.17 Å, respectively (Figure 16c). The primary differences among the members of this series are localized to the peripheral residues. It is not entirely clear that a fair comparison can be drawn between **31** and the other members of the homologous *i*+2 series, all of which are Leu-containing at the *i*+3 position. The *i*+3 Phe residue of **31** may not be structurally innocent, as we have not observed prehelical secondary structures for peptides with benzylic *i*+3 residues. It is possible that the type I′ double β-turn geometry is more favorable when the *i*+3 residue is alkyl-substituted.

Amide plane flipping is known to interconvert types II and I β-turns in proteins via a relatively low-barrier, concerted rotation about $\psi(i+1)$ and $\phi(i+2)$.[20] However, the type I′ β-turns we have observed would require a more global conformational change to access the observed, prehelical structures from the intended type II′ β-hairpins. This includes significant reorganization of the peripheral residues and side-chains. Only a few similar structures are reported in the CSD, most of which are found within cyclic peptides.[64] Furthermore, the documentation of this unexpected structure in solution provides evidence that this conformation is important to consider, at least for this class of peptide-based catalysts.

C-Terminal Cap. An often-overlooked structural attribute of these peptides is the *C*-terminal protecting group (cap). In the course of optimizing peptide-based catalysts for a wide variety of enantioselective reactions, we have encountered multiple scenarios in which the choice of *C*-terminal cap proved essential to achieve high levels of enantioinduction.[9,14,20,28] In cases where *N*,*N*-dimethyl amides outperformed the corresponding methyl esters, the enhanced selectivity has been ascribed to a stabilization of the β-hairpin structure via a more favorable N–H(i)···O(i+3) H-bond, since amides tend to be better H-bond acceptors than esters.[65] As such, we wondered if the *C*-terminal cap might influence the distribution of secondary structures within our library. Figure 17a summarizes these data.[62] Methyl

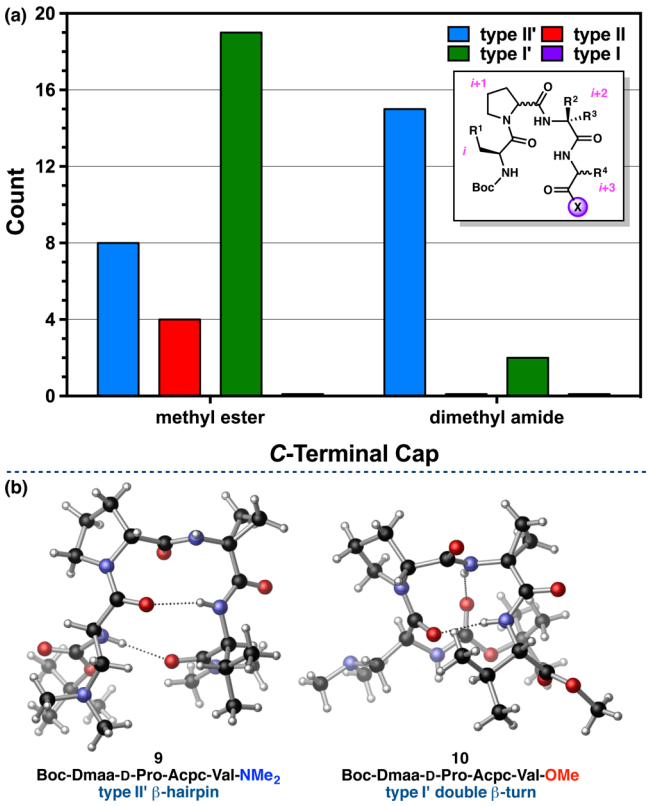

Figure 17. (a) Occurrence of canonical turn-motifs as a function of the *C*-terminal cap. Peptides **32** and **35**–**37** were excluded from this analysis. (b) Homologues **9** and **10** differ only in their *C*-terminal cap, and yet they exhibit different secondary structures.

esters comprise nearly 65% of the tetrapeptides analyzed, and *N*,*N*-dimethyl amides make up the remaining 35%. Despite the population imbalance, there seems to be a difference between the two types of *C*-terminal caps. While the *N*,*N*-dimethyl amides contain a high type II′/I′ ratio, the conformational landscape of the methyl esters is more even, yet still skewed in favor of the prehelical, type I′ β-turn structures. Thus, it seems that the dimethyl amide cap does indeed stabilize type II′ β-turns to some degree. Of the 15 type II′ amides, 13 (87%) are

DOI: 10.1021/jacs.6b11348
J. Am. Chem. Soc. 2017, 139, 492–516

β-hairpins. As a side note, no L-Pro-containing peptides with dimethyl amide caps were analyzed, hence the lack of type II β-turns in amide bin.

Additional insight may be gleaned from structural comparisons of homologous pairs. The example of peptides **3** and **4**, for instance, suggests that the change from *N*,*N*-dimethyl amide to methyl ester within an otherwise identical sequence changes the conformational landscape in favor of the prehelical geometry. The *N*,*N*-dimethyl amide variant (**3**) exists as both type II′ β-hairpins (**3a**,**b**) and type I′ double β-turns (**3c**) in the solid state, while methyl ester-containing **4** only exhibits the type I′ structure across the five symmetry-independent molecules examined. These solid-state observations are mirrored in the NMR solution structures, as well. The same trend was observed in Acbc-containing peptides **16** and **17**. In the case of peptides **9** and **10**, only one conformer of each was observed in the solid state, with *N*,*N*-dimethyl amide **9** adopting a type II′ β-hairpin and methyl ester **10** as a prehelical type I′ β-turn (Figure 17b). These data provide evidence in support of our previous hypothesis that *N*,*N*-dimethyl amide caps tend to favor nucleation of β-hairpin structures. Nevertheless, it is important to acknowledge the exceptions that we observed. The crystal structures of homologues **12** and **13** do not support this hypothesis, nor do those of peptides **24** and **25** (Chart 1). All of these crystal structures exhibit type II′ β-hairpin geometries despite the differences in *C*-terminal cap (Figures S3.12−S3.13 and S3.25−S3.26).

In terms of the influence of the *C*-terminal cap on the observed enantioselectivity in the bromination of quinazolinone **1** (eq 2), the effects appear to be subtle and context-dependent. While the *N*,*N*-dimethyl amides indeed prove to be superior to the methyl esters in lower-selectivity regimes (e.g., 75:25 vs 67:33 er with **24** and **25**, respectively),[28a] this trend did not necessarily hold within the more selective catalyst series.[28b] In fact, examination of the methyl ester variant of **3** led to the discovery of **4**, which was both more reactive and selective. However, *N*,*N*-dimethyl amide-containing **16** was modestly more selective than methyl ester-containing **17** (85:15 vs 83:17 er), suggesting that the effect of the *N*-terminal cap is modulated by the *i*+2 residue. The *i*+3 residue also seems to influence the end-cap effects, even when Acpc is incorporated at the *i*+2 position. For example, Val-containing amide **9** is more selective than its ester variant **10** (94:6 vs 91:9), and Phe-containing amide **12** is more selective than ester **13** (88:12 vs 86:14 er). Thus, it seems that the methyl esters may be beneficial above some selectivity threshold, especially when paired with Leu at the *i*+3 position. Structurally, it seems plausible that a weakened N−H(*i*)···O(*i*+3) β-hairpin H-bond[65] could produce a significant geometric change, especially when paired with backbone conformational driving forces, such as the more helical tendencies of Acpc. Another factor that should be considered in this context is that tertiary amides are known to catalyze electrophilic bromination reactions.[66] Thus, depending on the disposition of the other amides within the peptide scaffold, the enantioselectivity could be altered by the presence or absence of a *C*-terminal *N*,*N*-dimethyl amide; one might envision this to be either beneficial or deleterious to enantioselectivity depending on the overall conformation of the catalyst.

L-Pro Series. Thus far, the discussion has primarily focused on the D-Pro-containing sequences that comprise a majority (83%) of this structure library. These sequences have been observed to nucleate "mirror image" β-turns (types I′ and II′) in the solid state and in solution. However, the remaining 17% of this library are L-Pro-containing peptides, which are predisposed toward types I and II β-turns. Of the six entries, five are characterized as type II β-turns (**15**, **21**, **30**, **35**−**36**), while only a single type I turn (**37**) is observed (Chart 1). According to the work of Gellman and co-workers, β-hairpin structures are generally disfavored in this class of homochiral (i.e., all L-containing) peptides relative to the corresponding heterochiral (e.g., D-Pro-containing at *i*+1) peptides.[11a] This is often attributed to incompatibility between the twist of the antiparallel strands with that of the type I or II loop-region.[3,35] The result is that L-homochiral peptides equilibrate between β- and γ-turn geometries (Figure 2c). Our findings in the solid state and in solution support these observations.

Crystallographic Analysis of Homologous L-Pro Series. We were able to obtain X-ray data for a homologous series of L-Pro-containing peptides with the sequence Boc-Dmaa-Pro-Xaa-Leu-OMe (Figure 18), allowing further comparisons to be drawn to

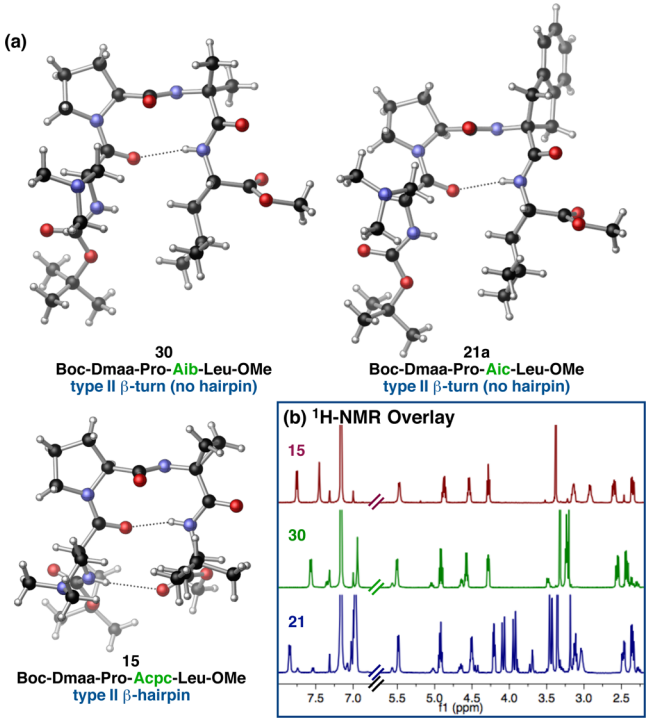

Figure 18. (a) Homologous series of L-Pro-containing peptides differing from one another only in the *i*+2 residue. Only one symmetry-independent conformer of **21** is shown (**21a**). (b) Stacked ^{1}H NMR spectra of the peptides shown in (a) acquired under identical conditions (600 MHz, 0.01 M in C_6D_6, 20−24 °C).

the D-Pro variants discussed previously (Figure 15a). The Aib-containing peptide **30** exhibits a type II β-turn in the solid state (Figure 18a). The *i*+3 residue is oriented such that a β-hairpin H-bond is not possible, in keeping with the previous studies of homochiral sequences.[11a,35] The D-Pro variant of **30**, peptide **25**, does adopt a β-hairpin structure in the solid state (Figure 15a). The Aic-containing peptide **21** demonstrates these same overall structural features as **30** in both symmetry-independent molecules (**21a**, Figure 18a). This is in direct contrast to the D-Pro variants, peptides **19a** and **19b**, which nucleate prehelical, type I′ β-turns in the solid state (Figure 9). It is notable that no intermolecular H-bonds to the "free" methyl ester moiety are observed in **30** or **21** (Table S4.41). This suggests that the

DOI: 10.1021/jacs.6b11348
J. Am. Chem. Soc. 2017, 139, 492−516

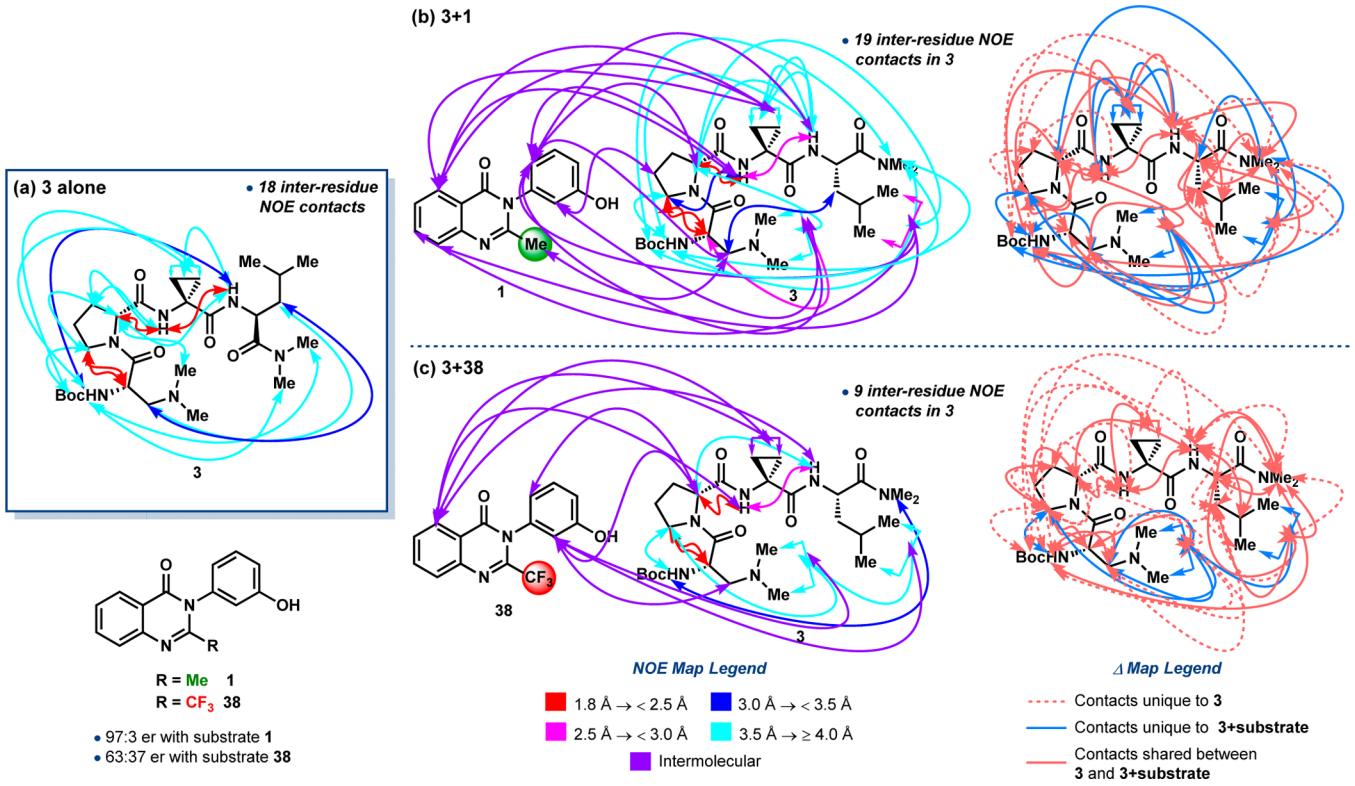

Figure 19. Measured NOE correlations for (a) peptide **3** alone, (b) a 1:1 mixture of **3** + **1**, and (c) a 1:1 mixture of **3** + **38** (600 MHz, 0.01 M, C_6D_6, 25 °C). The NOE maps show the inter-residue NOE's of peptide **3** and the intermolecular NOE's between **3** and the titrated substrate. The Δ maps show how the NOE contacts change as a function of presumed substrate binding. The data are consistent with a more defined complex **3** + **1**, while **3** + **38** is less rigid.

absence of a hairpin is not the result of lattice effects, but rather it reflects the conformational preferences of this class of peptides.

Surprisingly, a type II β-hairpin structure is observed for the L-Pro-Acpc-containing peptide **15** (Figure 18a). The N−H(i)···O(i+3) hairpin H-bond is directional, with an N−H(i)···O(i+3) angle of 165(6)°, but the N(i)···O(i+3) distance is at the upper limit of what might be considered an H-bonding interaction, measuring 3.243(6) Å. For context, the average hairpin N···O length and N−H···O angle are 2.986 ± 0.148 Å and 162 ± 9°, respectively, over all hairpins in the library. DFT optimization of **15** did not shorten the N(i)···O(i+3) distance appreciably (Figure S6.07). These data suggest that the N−H(i)···O(i+3) H-bond of **15** is likely quite weak owing to the conformational pressures that tend to destabilize such interactions in short sequence β-hairpins. The D-Pro variant of **15**, peptide **4**, was found to exhibit the prehelical, type I′ β-turn structure in the solid state and in solution (Figure 7). This observation further underscores the uniqueness of Acpc, in that it has been found to exist within conformations, such as the type II β-hairpin of **15** and the prehelical, type I′ β-turn of **4**, that have been observed less frequently. Overall, compensatory interactions may lead to the accommodation of otherwise unusual conformational profiles.

NMR Analysis of Homologous L-Pro Series. The solid-state observations of this L-Pro-series are largely recapitulated in solution. The ^{1}H NMR spectra of **30** and **21** show some conformational heterogeneity; a set of minor (~20%) peaks is observed for both peptides, which is consistent with a slow-exchange conformational equilibrium on the NMR time-scale (Figures 19b). While it is possible that this heterogeneity describes the equilibrium between β- and γ-turn structures, the interconversion of these forms is expected to be a fast exchange phenomenon in the context of Pro-Xaa turns,[11a] in which both H-bonded states are readily accessible and can interconvert with low barriers. Perhaps a more likely scenario is Pro *trans*/*cis* isomerization, which could be sufficiently slow on the NMR time scale to allow for the observation of discrete signals.[67] This would intimate that peptides **30** and **21** equilibrate between well folded (*trans* Pro) and unfolded or loosely folded (*cis* Pro) states in solution as a function of their homochiral sequences. Although a heterochiral sequence, the X-ray crystal structure of peptide **32** provides an example of an unfolded *cis*-Pro rotamer (Figure S3.33). The spectrum of peptide **15**, on the other hand, shows only one set of peaks, which may be attributed to either fast exchange of conformers or stabilization of a single, low-energy conformer. In light of our findings for similar peptides, especially the D-Pro-Acpc variants (e.g., **4**), the former is a more plausible explanation. The relatively downfield chemical shift of the N*H*(Acpc) signal suggests that **15** samples β- and γ-turn conformations in solution.

Based on additional NMR analyses, the data for peptide **15** and the major rotamers of peptides **21** and **30** are consistent with type II β-turn conformations in solution (0.01 M, C_6D_6, 20−24 °C). The $\phi(i)$ values calculated from $^3J_{NH-H\alpha}$ for all three peptides are tightly clustered: − 86° or −154° for **15**, −82° or −158° for **21**, and −89° or −151° for **30** (Table S5.40). On the other hand, the calculated $\phi(i+3)$ dihedrals of **15** and **21** are both of −89° or −142°, while the those of **30** are −89° or −151°. These $\phi(i)$ and $\phi(i+3)$ values fit within the ranges expected in the proposed type II β-turns (Figure S5.15). Comparing the ^{1}H NMR spectra, the L-Pro-containing peptides

DOI: 10.1021/jacs.6b11348
J. Am. Chem. Soc. 2017, 139, 492−516

are different from the corresponding D-Pro-containing variants (Figure S5.17). For example, the N*H*(Leu), N*H*(Acpc), and N*H*(Dmaa) resonances are all noticeably upfield-shifted in **15** relative to **4**, especially with regard to the N*H*(Dmaa) signal (Table S5.41). In peptide **21**, the N*H*(Leu) signals are essentially equal to those of D-Pro-containing **19**, whereas those of N*H*(Aic) and N*H*(Dmaa) are both nearly 0.3 ppm upfield-shifted. On the other hand, only the N*H*(Dmaa) resonance of peptide **30** is upfield-shifted, while the N*H*(Leu) and N*H*(Aib) chemical shifts are essentially equal to those of **25**. These differences represent changes in the intramolecular H-bonding network that disfavor β-hairpin formation via the N−H(i)···O(i+3) H-bond in the L-Pro-containing peptides. Additionally, the upfield chemical shifts observed for the N*H*(i+2) signals in peptides **21** and **30** likely signify a solvent-exposed state, while the same signal remains moderately downfield-shifted in **15**. The NOESY spectrum of peptide **15** shows N*H*(Dmaa) ↔ δ(Leu), N*H*(Acpc) ↔ N*H*(Leu), N*H*(Leu) ↔ α(Pro), and δ(Leu) ↔ α(Pro) NOE contacts, in addition to a very strong α(Pro) ↔ N*H*(Acpc) correlation (Figure S5.04). All of these data align with a type II β-turn/γ-turn conformational equilibrium in solution. Interestingly, neither gas phase DFT optimization nor solution phase NMR analysis provide evidence for the N−H(i)···O(i+3) hairpin H-bond observed in the crystal structure of **15**. In peptide **21**, the NOESY spectrum reveals a few relevant NOEs, including N*H*(Dmaa) ↔ β(Leu) and N*Me*$_2$(Dmaa) ↔ β(Aic) correlations (Figure S5.09). Despite the absence of an α(Pro) ↔ N*H*(Aic) crosspeak, the cumulative NMR data support a nonhairpin type II β-turn conformation in solution, similar to the crystal structure of **21**. Peptide **30** also shares this assignment, which is supported by O*Me*(Leu) ↔ N*H*(Aib) and N*H*(Aib) ↔ β(Dmaa) NOE contacts, as well as a very strong α(Pro) ↔ N*H*(Aib) correlation (Figure S5.12).

Connection to Enantioselective Catalysis in the Homologous L-Pro Series. Peptide **15** is a highly enantioselective catalyst for the bromination reaction presented in eq 2, delivering tribromide **2** in 11:89 er in favor of the opposite enantiomer provided by peptide **4**, its Pro-Cα epimer.[28b] In other reactions we have studied employing Pro-Xaa-type catalysts, changes from D- to L-Pro (or *vice versa*) within an otherwise identical catalyst sequence typically provide lower enantioselectivity in favor of the opposite enantiomer.[9a] Indeed, peptides **21** and **30** follow this trend relative to their D-Pro variants; both **21** and **30** provide tribromide ***ent*-2** in 45:55 er. Thus, the high level of enantiodivergence observed using Acpc-containing catalyst **15** is rather unusual, and it suggests that enantioinduction is primarily dictated by the turn sense. These findings are particularly intriguing in light of the structural observations of this homologous series. Of the three L-Pro-containing peptides examined, only peptide **15** adopts a well-folded conformation in the solid-state and in solution, while **21** and **30** are partially unfolded in solution owing to the minor population of *cis*-Pro rotamer (Figure 18b). Perhaps this apparent structural homogeneity is partially responsible for the enhanced selectivity of **15** relative to its i+2 homologues. While more folded than **21** and **30** on average, **15** also shows NOEs consistent with more than one folded state, notably β- and γ-turn conformations. Thus, conformational dynamics are possibly involved in the enhanced selectivity of **15**.

Further Connections to Enantioselective Catalysis—Catalyst−Substrate Titration Studies. It is important to emphasize that the specific mechanism of Lewis base- and Brønsted base-catalyzed bromination of arenes is not definitively known in terms of the bond forming steps.[66] Nevertheless, we are able to glean additional information relevant to catalysis by analyzing the solution structures of peptides in the presence of substrates.[32a] We thus examined catalyst-substrate mixtures employing NMR techniques. In particular, we compared the solution structure of catalyst **3** to those of 1:1 mixtures that also contained either a very good substrate (**3** + **1**) or a poor substrate (**3** + **38**) for the atroposelective bromination reaction described in eq 1.[28a] Each sample was prepared and analyzed using the same approach employed for peptide **3** alone (600 MHz, 0.01 M in C_6D_6, 25 °C). However, due to the difficulty in extracting $^3J_{NH-H\alpha}$ values for the i and i+3 residues of **3** in mixtures **3** + **1** and **3** + **38**,[68] as well as the differential impacts of substrate anisotropy on the chemical shits of **3**, only the NOE data provide a straightforward interpretation. Comparison of the data acquired for **3** + **1** and **3** + **38** to each other and to that of peptide **3** alone reveals significant deviations in catalyst conformation as a function of association. The NOE contacts from the ^{1}H−^{1}H-NOESY spectra of **3**, **3** + **1**, and **3** + **38** are presented in Figure 19.

As discussed previously, the solution NMR data acquired for peptide **3** are most consistent with a type II′ β-hairpin structure that is possibly in flux with prehelical, type I′ β-turn forms. This assignment was made on the basis of 18 inter-residue NOE correlations (Figure 19a). Upon titration of quinazolinone **1**, we observe a change in the NOESY spectrum of **3** that is consistent with a conformational change induced by substrate association. Mixture **3** + **1** exhibits 19 inter-residue NOEs, 13 of which are unique to **3** + **1** and are not observed in **3** alone. In addition, 15 intermolecular contacts between **3** and **1** are observed (Figure 19b). We also note that the ^{1}H-resonance corresponding to N*H*(Acpc) shifts downfield by 0.93 ppm, which may implicate this amide in substrate docking.[28a] These through-space interactions suggest that **3** associates with quinazolinone **1** in a rigid type II′ β-hairpin conformation. This assignment is significantly less ambiguous than that of **3** alone, and is supported by α(D-Pro) ↔ N*H*(Acpc), β(Dmaa) ↔ β(Leu), and N*H*(Dmaa) ↔ δ(Leu) NOEs, as well as the α(D-Pro) ↔ δ(Leu), Boc(Dmaa) ↔ N*Me*$_2$(Leu), and N*H*(Acpc) ↔ β(Acpc) NOEs unique to **3** + **1**. In contrast, titration of quinazolinone **38** produces changes in the NOESY spectrum of **3** that are consistent with both a less defined folded state and a looser catalyst-substrate association (Figure 19c). The NOESY spectrum of **3** + **38** shows only nine inter-residue correlations, five of which are unique to the mixture. The strong α(D-Pro) ↔ N*H*(Acpc) and long-range N*Me*$_2$(Dmaa) ↔ δ(Leu) NOEs support a type II′ β-hairpin conformation of **3** + **38**, although the notably reduced quantity of through-space interactions relative to **3** + **1** suggest that the structure less rigid and possibly fluxional. Moreover, fewer intermolecular NOE contacts are observed between **3** and **38**, and these nine correlations provide less coverage of the whole quinazolinone scaffold than in **3** + **1**. Although N*H*(Acpc) also shifts significantly downfield (by 0.88 ppm) in **3** + **38**, the data are consistent with a weaker interaction between **3** and **38** or perhaps multiple, interconverting binding orientations.

The emergent picture is one that suggests a higher degree of structural organization, and perhaps a more homogeneous conformation, for catalyst **3** as it associates with a good substrate (**1**). On the other hand, in the presence of a poor substrate (**38**), the conformational profile of **3** becomes even

DOI: 10.1021/jacs.6b11348
J. Am. Chem. Soc. 2017, 139, 492−516

more ambiguous than **3** alone. These observations are consistent with the induced fit model that is well characterized for allosteric enzymes as they associate with their substrates[69] and underscores the importance of dynamics in peptide-catalyzed, enantioselective reactions.

CONCLUSIONS

Our data show that a wide range of conformational states is available to low-molecular-weight tetrapeptides. In the solid state, multiple conformations of the same peptide sequence are manifest in a high incidence of symmetry-independent conformers and polymorphs within this structure library. Interpretations of NMR data are repeatedly compatible with various populated states in solution. On its own, this situation could be claimed to be unsurprising—short peptides are flexible and occupy shallow conformational energy landscapes. Yet, the direct experimental observation of allowable conformations in the solid state and in solution is rare. Moreover, the discovery and application of residue-specific conformational biases for nucleation of secondary structures remain an important tenet of peptide and protein design. These preferences are, of course, context dependent. The results reported herein, including redundant structural analyses of identical sequences and similar analyses of many related analogs employing both X-ray diffraction and NMR methods, culminate in the direct observation of multiple conformational states, and provide an aggregate of data that reveal a high level of variation. We find the level of diversity among peptides biased toward similar structural motifs to be striking. In response, computational analysis has allowed an assessment of relative energies for experimentally observed states, expanding intuition about the complex equilibria available to simple, folded peptides.

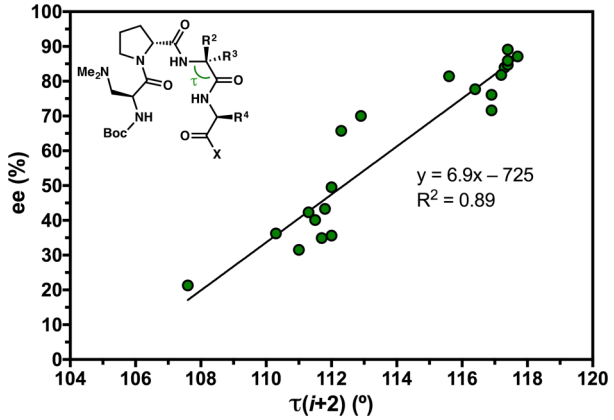

Figure 20. Linear correlation between $\tau(i+2)$ and ee of tribromide **2** observed for the reaction shown in eq 2. For structures with more than one symmetry-independent conformer, the average $\tau(i+2)$ value was used. Additional details are provided in the Supporting Information.

What emerges is a database of structural information that illuminates the conformational space available to these peptides, many of which are known to be catalysts for enantioselective reactions. What are the key structural elements that allow these low-molecular-weight, acyclic peptides to function as enantioselective catalysts? It seems that there are likely many, and the importance of catalyst dynamics is often one.[32] The analysis of structural information from peptide-based catalyst libraries may also allow for the identification of correlations between structural features and enantioselectivity.[70] For example, Figure 20 shows a rather good correlation (R^2 = 0.89) between enantioselectivity (ee) in the atroposelective bromination of quinazolinone **1** (eq 2) and the crystallographic τ-angle of the i+2 position in a particular subset of this catalyst library.[28] This factor was not among the design considerations when the catalyst library was conceived, and its connection to the observed enantioselectivity is not fully understood. Is it causative or coincidental? The recognition of this provocative trend from the structural database, combined with an improved, experimentally and computationally grounded appreciation for the catalyst conformational profiles, better positions future studies of flexible, peptide-based catalysts to be hypothesis driven.

ASSOCIATED CONTENT

Supporting Information

The Supporting Information is available free of charge on the ACS Publications website at DOI: 10.1021/jacs.6b11348.

Synthetic methods, characterization, X-ray crystallographic data, and solution NMR data for peptides **3**–**37**, as well as additional analyses of structural trends and DFT computational data (PDF)

CIF data for **3a,b** (1412920), **3c** (1453125), **4a** (1453124), **4b–e**, **5**, **6**, **7a,b**, **8**, **9**, **10**, **11**, **12**, **13**, **14**, **15**, **16a,b**, **16c**, **17a,b**, **18a,b**, **19a,b**, **20a,b**, **21a,b**, **22a,b**, **23**, **24**, **25**, **26**, **27**, **28**, **29a,b**, **30**, **31**, **32a,b**, and **33a,b** (ZIP)

AUTHOR INFORMATION

Corresponding Author

*scott.miller@yale.edu

ORCID

Scott J. Miller: 0000-0001-7817-1318

Notes

The authors declare no competing financial interest.

Crystallographic data are deposited with the Cambridge Crystallographic Data Centre (CCDC) under the following accession numbers: **4b–e** (1510507), **5** (1510503), **6** (1510502), **7a,b** (1510506), **8** (1510504), **9** (1510505), **10** (1510508), **11** (1510516), **12** (1510513), **13** (1510509), **14** (1510514), **15** (1510510), **16a,b** (1510512), **16c** (1510511), **17a,b** (1510515), **18a,b** (1510517), **19a,b** (1510525), **20a,b** (1510518), **21a,b** (1510519), **22a,b** (1510522), **23** (1510526), **24** (1510521), **25** (1510520), **26** (1510524), **27** (1510523), **28** (1510530), **29a,b** (1510527), **30** (1510531), **31** (1510528), **32a,b** (1510529), and **33a,b** (1510532).

ACKNOWLEDGMENTS

We would like to thank Byoungmoo Kim, Michael Giuliano, Alex Chinn, Christopher Shugrue, David Romney, William Jorgensen, Julian Tirado-Rives, and Matthew Diener for helpful discussions and insightful comments, as well as Guillaume Pelletier, Kimberly Barrett, and Newlyn Joseph for materials and data. A.J.M. gratefully acknowledges early support from the National Science Foundation Graduate Research Fellowship Program. All computational work was supported by the facilities and staff of the Yale University Faculty of Arts and Sciences High Performance Computing Center, and by the National Science Foundation under grant number CNS 08-21132, that partially funded acquisition of the facilities. We would also like to thank Simon Teat of the Advanced Light

DOI: 10.1021/jacs.6b11348
J. Am. Chem. Soc. 2017, 139, 492–516

Source (ALS), Lawrence Berkeley National Laboratory, for acquiring some X-ray crystal data presented herein. The ALS is supported by the Director, Office of Science, Office of Basic Energy Sciences, of the U.S. Department of Energy under Contract Number DE-AC02-05CH11231. We are grateful to the National Institute of General Medical Sciences of the NIH (GM-068649 and GM-096403) for support.

REFERENCES

(1) (a) Knowles, J. R. *Nature* **1991**, *350*, 121−124. (b) Kirby, A. J. *Angew. Chem., Int. Ed. Engl.* **1996**, *35*, 706−724. (c) Smith, A. J. T.; Müller, R.; Toscano, M. D.; Kast, P.; Hellinga, H. W.; Hilvert, D.; Houk, K. N. *J. Am. Chem. Soc.* **2008**, *130*, 15361−15373. (d) Creighton, T. E. *Proteins: Structures and Molecular Properties*, 2nd ed.; W. H. Freeman & Co.: New York, 1993.

(2) (a) Baker, D. *Nature* **2000**, *405*, 39−42. (b) Dobson, C. M.; Šali, A.; Karplus, M. *Angew. Chem., Int. Ed.* **1998**, *37*, 868−893. (c) Valentine, J. S., Ed. *Acc. Chem. Res.* **1998**, *31*, 697 (Protein Folding Special Issue).

(3) (a) Wilmot, C. M.; Thornton, J. M. *J. Mol. Biol.* **1988**, *203*, 221−232. (b) Hutchinson, E. G.; Thornton, J. M. *Protein Sci.* **1994**, *3*, 2207−2216.

(4) For reviews on synthetic foldamers, see: (a) Guichard, G.; Huc, I. *Chem. Commun.* **2011**, *47*, 5933−5941. (b) Goodman, C. M.; Choi, S.; Shandler, S.; DeGrado, W. F. *Nat. Chem. Biol.* **2007**, *3*, 252−262. (c) Venkatraman, J.; Shankarama, S. C.; Balaram, P. *Chem. Rev.* **2001**, *101*, 3131−3152. (d) Hill, D. J.; Mio, M. J.; Prince, R. B.; Hughes, T. S.; Moore, J. S. *Chem. Rev.* **2001**, *101*, 3893−4012. (e) Gellman, S. H. *Curr. Opin. Chem. Biol.* **1998**, *2*, 717−725.

(5) For select examples of peptide-based dynamic foldamers and molecular devices, see: (a) Le Bailly, B. A. F.; Clayden, J. *Chem. Commun.* **2016**, *52*, 4852−4863. (b) Mazzier, D.; Crisma, M.; De Poli, M.; Marafon, G.; Peggion, C.; Clayden, J.; Moretto, A. *J. Am. Chem. Soc.* **2016**, *138*, 8007−8018. (c) Brown, R. A.; Diemer, V.; Webb, S. J.; Clayden, J. *Nat. Chem.* **2013**, *5*, 853−860. (d) Lewandowski, B.; De Bo, G.; Ward, J. W.; Papmeyer, M.; Kuschel, S.; Aldegunde, M. J.; Gramlich, P. M.; Heckmann, D.; Goldup, S. M.; D'Douza, D. M.; Fernandes, A. E.; Leigh, D. A. *Science* **2013**, *339*, 189−193. (e) Meillon, J.-C.; Voyer, N.; Biron, É.; Sanschagrin, F.; Stoddart, J. F. *Angew. Chem., Int. Ed.* **2000**, *39*, 143−145. (f) Dado, G. P.; Gellman, S. H. *J. Am. Chem. Soc.* **1993**, *115*, 12609−12610.

(6) Miller, S. J. *Acc. Chem. Res.* **2004**, *37*, 601−610.

(7) For reviews, see: (a) Lewandowski, B.; Wennemers, H. *Curr. Opin. Chem. Biol.* **2014**, *22*, 40−46. (b) Wennemers, H. *Chem. Commun.* **2011**, *47*, 12036−12041. (c) Colby Davie, E. A.; Mennen, S. M.; Xu, Y.; Miller, S. J. *Chem. Rev.* **2007**, *107*, 5759−5812.

(8) For a review, see: (a) Revell, J. D.; Wennemers, H. *Curr. Opin. Chem. Biol.* **2007**, *11*, 269−278. For select examples, see: (b) Lichtor, P. A.; Miller, S. J. *ACS Comb. Sci.* **2011**, *13*, 321−326. (c) Copeland, G. T.; Miller, S. J. *J. Am. Chem. Soc.* **1999**, *121*, 4306−4307.

(9) For select examples, see: (a) Jarvo, E. R.; Copeland, G. T.; Papaioannou, N.; Bonitatebus, P. J.; Miller, S. J. *J. Am. Chem. Soc.* **1999**, *121*, 11638−11643. (b) Peris, G.; Jakobsche, C. E.; Miller, S. J. *J. Am. Chem. Soc.* **2007**, *129*, 8710−8711.

(10) For early studies of β-turns in proteins, see: (a) Rose, G. D.; Gierasch, L. M.; Smith, J. A. *Adv. Protein Chem.* **1985**, *37*, 1−109. (b) Richardson, J. S. *Adv. Protein Chem.* **1981**, *34*, 167−339. (c) Wilmot, C. M.; Thornton, J. M. *Protein Eng., Des. Sel.* **1990**, *3*, 479−493. (d) Lewis, P. N.; Momany, F. A.; Scheraga, H. A. *Biochim. Biophys. Acta, Protein Struct.* **1973**, *303*, 211−229.

(11) (a) Haque, T. S.; Little, J. C.; Gellman, S. H. *J. Am. Chem. Soc.* **1996**, *118*, 6975−6985. (b) Liang, G.-B.; Rito, C. J.; Gellman, S. H. *J. Am. Chem. Soc.* **1992**, *114*, 4440−4442. (c) Jiménez, A. I.; Cativiela, C.; Aubry, A.; Marraud, M. *J. Am. Chem. Soc.* **1998**, *120*, 9452−9459. (d) Boussard, G.; Marraud, M. *J. Am. Chem. Soc.* **1985**, *107*, 1825−1828. (e) Ravi, A.; Venkataram Prasad, B. V.; Balaram, P. *J. Am. Chem. Soc.* **1983**, *105*, 105−109.

(12) (a) Sibanda, B. L.; Thornton, J. M. *Nature* **1985**, *316*, 170−174. (b) Sibanda, B. L.; Blundell, T. L.; Thornton, J. M. *J. Mol. Biol.* **1989**, *206*, 759−777. (c) Blanco, F. J.; Jiménez Angeles, M.; Herranz, J.; Rico, M.; Santoro, J.; Nieto, J. L. *J. Am. Chem. Soc.* **1993**, *115*, 5887−5888.

(13) For discussions of H-bonding as it pertains to catalysis, see: (a) Knowles, R. R.; Jacobsen, E. N. *Proc. Natl. Acad. Sci. U. S. A.* **2010**, *107*, 20678−20685. (b) Simón, L.; Goodman, J. M. *J. Org. Chem.* **2010**, *75*, 1831−1840. (c) Bernardi, L.; Fochi, M.; Comes Franchini, M.; Ricci, A. *Org. Biomol. Chem.* **2012**, *10*, 2911−2922. (d) Mader, M. M.; Bartlett, P. A. *Chem. Rev.* **1997**, *97*, 1281−1301.

(14) (a) Copeland, G. T.; Jarvo, E. R.; Miller, S. J. *J. Org. Chem.* **1998**, *63*, 6784−6785. (b) Cowen, B. J.; Saunders, L. B.; Miller, S. J. *J. Am. Chem. Soc.* **2009**, *131*, 6105−6107. (c) Metrano, A. J.; Miller, S. J. *J. Org. Chem.* **2014**, *79*, 1542−1554.

(15) For ease of reference, we provide definitions of the following structural parameters discussed throughout the manuscript: ϕ, the backbone dihedral defined for rotation about C′−N−Cα−C′; ψ, the backbone dihedral defined for rotation about N−Cα−C′−N; ω, the backbone dihedral defined for rotation about Cα−C′−N−Cα, which, due to the planarity of the amide (C′−N) bond, is typically either 0° or 180°; χ_1, the side-chain dihedral defined for rotation about N−Cα−Cβ−Cγ; and τ, the N−Cα−C′ main-chain angle.

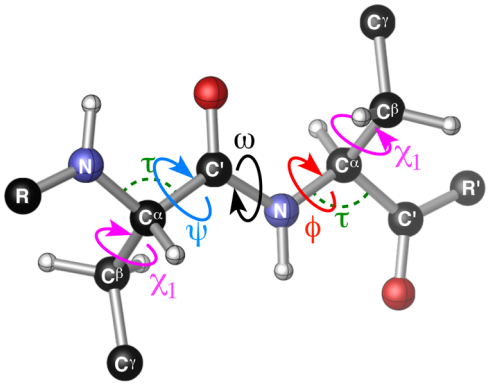

(16) For reviews on β-turns in biological and medicinal contexts, see: (a) Craik, D. J.; Fairlie, D. P.; Liras, S.; Price, D. *Chem. Biol. Drug Des.* **2013**, *81*, 136−147. (b) Robinson, J. A. *Acc. Chem. Res.* **2008**, *41*, 1278−1288. (c) Che, Y.; Books, B. R.; Marshall, G. R. *J. Comput.-Aided Mol. Des.* **2006**, *20*, 109−130. (d) Suat, K.; Jois, S. D. S. *Curr. Pharm. Des.* **2003**, *9*, 1209−1224. (e) Grauer, A.; König, B. *Eur. J. Org. Chem.* **2009**, *2009*, 5099−5111.

(17) For some examples of β-turn peptidomimetics, see: (a) Souers, A. J.; Ellman, J. A. *Tetrahedron* **2001**, *57*, 7431−7448. (b) Whitby, L. R.; Ando, Y.; Setola, V.; Vogt, P. K.; Roth, B. L.; Boger, D. L. *J. Am. Chem. Soc.* **2011**, *133*, 10184−10194. (c) Low, K. E.; Ler, S.; Chen, K. J.; Campbell, R. L.; Hickey, J. L.; Tan, J.; Scully, C. C. G.; Davies, P. L.; Yudin, A. K.; Zaretsky, S. *J. Med. Chem.* **2016**, *59*, 5403−5415. (d) Eckhardt, B.; Grosse, W.; Essen, L.-O.; Geyer, A. *Proc. Natl. Acad. Sci. U. S. A.* **2010**, *107*, 18336−18341. (e) Van der Poorten, O.; Knuhtsen, A.; Pedersen, D. S.; Battet, S.; Tourwé, D. *J. Med. Chem.* 2016, *ASAP*, DOI: 10.1021/acs.jmedchem.6b01029.

(18) (a) Gunasekaran, K.; Gomathi, L.; Ramakrishnan, C.; Chandrasekhar, J.; Balaram, P. *J. Mol. Biol.* **1998**, *284*, 1505−1516. (b) Hayward, S. *Protein Sci.* **2001**, *10*, 2219−2227.

(19) For examples of extended β-hairpin structures in short peptides, see: (a) Karle, I. L.; Awasthi, S. K.; Balaram, P. *Proc. Natl. Acad. Sci. U. S. A.* **1996**, *93*, 8189−8193. (b) Aravinda, S.; Harini, V. V.; Shamala, N.; Das, C.; Balaram, P. *Biochemistry* **2004**, *43*, 1832−1846. (c) Aravinda, S.; Raghavender, U. S.; Rai, R.; Harini, V. V.; Shamala, N.; Balaram, P. *Org. Biomol. Chem.* **2013**, *11*, 4220−4231.

(20) D-Pro-Aib examples: (a) Barrett, K. T.; Miller, S. J. *J. Am. Chem. Soc.* **2013**, *135*, 2963−2966. (b) Han, S.; Miller, S. J. *J. Am. Chem. Soc.* **2013**, *135*, 12414−12421. (c) Fowler, B. S.; Mikochik, P. J.; Miller, S. J. *J. Am. Chem. Soc.* **2010**, *132*, 2870−2871. (d) Saunders, L. B.;

DOI: 10.1021/jacs.6b11348
J. Am. Chem. Soc. 2017, 139, 492−516

Cowen, B. J.; Miller, S. J. *Org. Lett.* **2010**, *12*, 4800−4803. (e) Lewis, C. A.; Miller, S. J. *Angew. Chem., Int. Ed.* **2006**, *45*, 5616−5619. D-Pro-Acpc example: (f) Shugrue, C. R.; Miller, S. J. *Angew. Chem., Int. Ed.* **2015**, *54*, 11173−11176. D-Pro-Aic example: (g) Mbofana, C. T.; Miller, S. J. *J. Am. Chem. Soc.* **2014**, *136*, 3285−3292. L-Pro-Cle examples: (h) Fiori, K. W.; Puchlopek, A. L. A.; Miller, S. J. *Nat. Chem.* **2009**, *1*, 630−634.

(21) MacArthur, M. W.; Thornton, J. M. *J. Mol. Biol.* **1991**, *218*, 397−412.

(22) (a) Haque, T. S.; Little, J. C.; Gellman, S. H. *J. Am. Chem. Soc.* **1994**, *116*, 4105−4106. (b) Stanger, H. E.; Gellman, S. H. *J. Am. Chem. Soc.* **1998**, *120*, 4236−4237. (c) Raghothama, S. R.; Awasthi, S. K.; Balaram, P. *J. Chem. Soc., Perkin Trans. 2* **1998**, 137−143. (d) Yan, Y.; Tropsha, A.; Hermans, J.; Erickson, B. W. *Proc. Natl. Acad. Sci. U. S. A.* **1993**, *90*, 7898−7902.

(23) For reviews on γ-turns in proteins, see: (a) Crisma, M.; De Zotti, M.; Moretto, A.; Peggion, C.; Drouillat, B.; Wright, K.; Couty, F.; Toniolo, C.; Formaggio, F. *New J. Chem.* **2015**, *39*, 3208−3216. (b) Milner-White, E. J. *J. Mol. Biol.* **1990**, *216*, 385−397.

(24) (a) Toniolo, C.; Crisma, M.; Formaggio, F.; Peggion, C. *Biopolymers* **2001**, *60*, 396−419. (b) Toniolo, C.; Benedetti, E. *Macromolecules* **1991**, *24*, 4004−4009. (c) Fabiano, N.; Valle, G.; Crisma, M.; Toniolo, C.; Saviano, M.; Lombardi, A.; Isernia, C.; Pavone, V.; Di Blasio, B.; Pedone, C.; Benedetti, E. *Int. J. Pept. Protein Res.* **1993**, *42*, 459−465. (d) Toniolo, C.; Crisma, M.; Formaggio, F.; Benedetti, E.; Santini, A.; Iacovino, R.; Saviano, M.; Di Blasio, B.; Pedone, C.; Kamphuis, J. *Pept. Sci.* **1996**, *40*, 519−527.

(25) (a) Prasad, B. V. V; Balaram, H.; Balaram, P. *Biopolymers* **1982**, *21*, 1261−1273. (b) Formaggio, F.; Barazza, A.; Bertocco, A.; Toniolo, C.; Broxterman, Q. B.; Kaptein, B.; Brasola, E.; Pengo, P.; Pasquato, L.; Scrimin, P. *J. Org. Chem.* **2004**, *69*, 3849−3856.

(26) For discussions of "privileged" chiral scaffolds, see: (a) Yoon, T. P.; Jacobsen, E. N. *Science* **2003**, *299*, 1691−1693. (b) Karukurichi, K. R.; Fei, X.; Swyka, R. A.; Broussey, S.; Shen, W.; Dey, S.; Roy, S. K.; Berkowitz, D. B. *Sci. Adv.* **2015**, *1*, e1500066−20.

(27) For other examples of Pro-Xaa β-turns in asymmetric catalysts, see: (a) Greenfield, S. J.; Agarkov, A.; Gilbertson, S. R. *Org. Lett.* **2003**, *5*, 3069−3072. (b) Krattiger, P.; Kovàsy, R.; Revell, J. D.; Ivan, S.; Wennemers, H. *Org. Lett.* **2005**, *7*, 1101−1103. (c) Agarkov, A.; Greenfield, S. J.; Xie, D.; Pawlick, R.; Starkey, G.; Gilbertson, S. R. *Biopolymers* **2006**, *84*, 48−73. (d) Revell, J. D.; Wennemers, H. *Adv. Synth. Catal.* **2008**, *350*, 1046−1052. (e) Akagawa, K.; Akabane, H.; Sakamoto, S.; Kudo, K. *Org. Lett.* **2008**, *10*, 2035−2037. (f) Wiesner, M.; Revell, J. D.; Wennemers, H. *Angew. Chem., Int. Ed.* **2008**, *47*, 1871−1874. (g) Wiesner, M.; Revell, J. D.; Tonazzi, S.; Wennemers, H. *J. Am. Chem. Soc.* **2008**, *130*, 5610−5611. (h) Wiesner, M.; Neuburger, M.; Wennemers, H. *Chem.−Eur. J.* **2009**, *15*, 10103−10109. (i) Chen, P.; Qu, J. *J. Org. Chem.* **2011**, *76*, 2994−3004. (j) Wiesner, M.; Revell, J. D.; Wennemers, H. *Angew. Chem., Int. Ed.* **2013**, *52*, 7228−7232. (k) Liao, R.-Z.; Santoro, S.; Gotsev, M.; Marcelli, T.; Himo, F. *ACS Catal.* **2016**, *6*, 1165−1171. (l) Grünenfelder, C. E.; Kisunzu, J. K.; Wennemers, H. *Angew. Chem., Int. Ed.* **2016**, *55*, 8571−8574. (m) Ueda, A.; Umeno, T.; Doi, M.; Akagawa, K.; Kudo, K.; Tanaka, M. *J. Org. Chem.* **2016**, *81*, 6343−6356.

(28) (a) Diener, M. E.; Metrano, A. J.; Kusano, S.; Miller, S. J. *J. Am. Chem. Soc.* **2015**, *137*, 12369−12377. (b) Metrano, A. J.; Abascal, N. C.; Mercado, B. Q.; Paulson, E. K.; Miller, S. J. *Chem. Commun.* **2016**, *52*, 4816−4819.

(29) For peptide **34**: (a) Blank, J. T.; Miller, S. J. *Biopolymers* **2006**, *84*, 38−47. For peptide **35**, see ref 9a. For peptide **36**: (b) Jakobsche, C. E.; Peris, G.; Miller, S. J. *Angew. Chem., Int. Ed.* **2008**, *47*, 6707−6711. For peptide **37**: (c) Blank, J. T.; Guerin, D. J.; Miller, S. J. *Org. Lett.* **2000**, *2*, 1247−1249.

(30) A search of the Cambridge Structural Database (CSD) on 17 October 2016 returned 424 Pro-Xaa-containing peptides, about half of which were cyclic. Of the 191 noncyclic entries: (1) 54 contained α,α-disubstituted residues as Xaa; (2) 12 contained Acpc as Xaa; and (3) 19 were tetramers.

(31) For examples in the context of β-turns, see: (a) Karnes, M. A.; Schettler, S. L.; Werner, H. M.; Kurz, A. F.; Horne, W. S.; Lengyel, G. A. *Org. Lett.* **2016**, *18*, 3902−3905. (b) Burke, N. L.; DeBlase, A. F.; Redwine, J. G.; Hopkins, J. R.; McLuckey, S. A.; Zwier, T. S. *J. Am. Chem. Soc.* **2016**, *138*, 2849−2857. For related examples, see: (c) Fierman, M. B.; O'Leary, D. J.; Steinmetz, W. E.; Miller, S. J. *J. Am. Chem. Soc.* **2004**, *126*, 6967−6971. (d) Lawson, K. V.; Rose, T. E.; Harran, P. G. *Proc. Natl. Acad. Sci. U. S. A.* **2013**, *110*, E3753−E3760. See also ref 22d.

(32) (a) Abascal, N. C.; Miller, S. J. *Org. Lett.* **2016**, *18*, 4646−4649. (b) Alford, J. S.; Abascal, N. C.; Shugrue, C. R.; Colvin, S. M.; Romney, D. K.; Miller, S. J. *ACS Cent. Sci.* **2016**, *2*, 733−739. (c) Abascal, N. C.; Lichtor, P. A.; Giuliano, M. W.; Miller, S. J. *Chem. Sci.* **2014**, *5*, 4504−4511.

(33) Thiel, W. *Angew. Chem., Int. Ed.* **2014**, *53*, 8605−8613. Section 4.4 is particularly relevant.

(34) For discussion of 3_{10}-helices, see: Tonlolo, C.; Benedetti, E. *Trends Biochem. Sci.* **1991**, *16*, 350−353.

(35) This virtual dihedral (ϖ) was previously used to describe the twist of an oligopeptide biased toward a β-turn geometry. See: Gunasekaran, K.; Ramakrishnan, C.; Balaram, P. *Protein Eng., Des. Sel.* **1997**, *10*, 1131−1141.

(36) For reviews on DFT: (a) Pople, J. A.; Gill, P. M. W.; Johnson, B. G. *Chem. Phys. Lett.* **1992**, *199*, 557−560. (b) Parr, R. G.; Yang, W. *Density-Functional Theory of Atoms and Molecules*; Oxford University Press: Oxford, 1989. For M06-2X: (c) Zhao, Y.; Truhlar, D. G. *Theor. Chem. Acc.* **2008**, *120*, 215−241.

(37) For reviews on polymorphism, see: (a) Cruz-Cabeza, A. J.; Bernstein, J. *Chem. Rev.* **2014**, *114*, 2170−2191. (b) Nangia, A. *Acc. Chem. Res.* **2008**, *41*, 595−604.

(38) Wang, A. C.; Bax, A. *J. Am. Chem. Soc.* **1996**, *118*, 2483−2494.

(39) (a) Gardner, R. R.; Gellman, S. H. *J. Am. Chem. Soc.* **1995**, *117*, 10411−10412. (b) Gellman, S. H.; Dado, G. P.; Liang, G.-B.; Adams, B. R. *J. Am. Chem. Soc.* **1991**, *113*, 1164−1173.

(40) (a) Wider, G.; Macura, S.; Kumar, A.; Ernst, R. R.; Wüthrich, K. *J. Magn. Reson.* **1984**, *56*, 207−234. (b) Jeener, J.; Meier, B. H.; Bachmann, P.; Ernst, R. R. *J. Chem. Phys.* **1979**, *71*, 4546−4553. (c) Awasthi, S. K.; Raghothama, S.; Balaram, P. *Biochem. Biophys. Res. Commun.* **1995**, *216*, 375−381.

(41) The batch of peptide **16** that gave rise to polymorphs **16a,b** and **16c** was catalytically competent in the atroposelective bromination of **1** described in eq 1. Additionally, the NMR spectrum of **16** is consistent with protonated catalyst (see the Supporting Information). As such, it is unlikely that our stock of **16c** is protonated. The source of the HCl equivalents remains unclear, but we speculate that the **16a,b** crystal may have nucleated on a grain of adventitious, wet NaCl.

(42) For a computational study of cyclobutane puckering, see: Glendening, E. D.; Halpern, A. M. *J. Phys. Chem. A* **2005**, *109*, 635−642.

(43) Zhou, A. Q.; O'Hern, C. S.; Regan, L. *Protein Sci.* **2011**, *20*, 1166−1171.

(44) Grünenfelder, C. E.; Kisunzu, J. K.; Trapp, N.; Kastl, R.; Wennemers, H. *Biopolymers (Pept. Sci.)* 2016, *ASAP*, DOI: 10.1002/bip.22912.

(45) Steiner, T. *Acta Crystallogr., Sect. B: Struct. Sci.* **2000**, *B56*, 673−676.

(46) (a) Choi, S. H.; Guzei, I. A.; Spencer, L. C.; Gellman, S. H. *J. Am. Chem. Soc.* **2010**, *132*, 13879−13885. (b) Choi, S. H.; Guzei, I. A.; Spencer, L. C.; Gellman, S. H. *J. Am. Chem. Soc.* **2009**, *131*, 2917−2924.

(47) Thompson, H. P. G.; Day, G. M. *Chem. Sci.* **2014**, *5*, 3173−3182.

(48) For a discussion of amide pyramidalization in proteins, see: (a) MacArthur, M. W.; Thornton, J. M. *J. Mol. Biol.* **1996**, *264*, 1180−1195. For related examples, see: (b) Cruz-Cabeza, A. J.; Day, G. M.; Motherwell, W. D. S.; Jones, W. *Cryst. Growth Des.* **2006**, *6*, 1858−1866. (c) Alemán, C.; Jiménez, A. I.; Cativiela, C.; Pérez, J. J.; Casanovas, J. *J. Phys. Chem. B* **2005**, *109*, 11836−11841.

DOI: 10.1021/jacs.6b11348
J. Am. Chem. Soc. 2017, 139, 492−516

(49) For example, see: (a) Brock, C. P.; Minton, R. P. *J. Am. Chem. Soc.* **1989**, *111*, 4586−4593. (b) Pearson, A. D.; Mills, J. H.; Song, Y.; Nasertorabi, F.; Han, G. W.; Baker, D.; Stevens, R. C.; Schultz, P. G. *Science* **2015**, *347*, 863−867. (d) Romney, D. K.; Miller, S. J. *Science* **2015**, *347*, 829. See also ref 47.
(50) Ramachandran, G. N.; Ramakrishnan, C.; Sasisekharan, V. *J. Mol. Biol.* **1963**, *7*, 95−99.
(51) (a) Hinderaker, M. P.; Raines, R. T. *Protein Sci.* **2003**, *12*, 1188−1194. (b) Choudhary, A.; Gandla, D.; Krow, G. R.; Raines, R. T. *J. Am. Chem. Soc.* **2009**, *131*, 7244−7246. (c) Bartlett, G. J.; Choudhary, A.; Raines, R. T.; Woolfson, D. N. *Nat. Chem. Biol.* **2010**, *6*, 615−620.
(52) (a) Duddy, W. J.; Nissink, J. W. M.; Allen, F. H.; Milner-White, E. J. *Protein Sci.* **2004**, *13*, 3051−3055. (b) Abbadi, A.; Mcharfi, M.; Aubry, A.; Premilat, S.; Boussard, G.; Marraud, M. *J. Am. Chem. Soc.* **1991**, *113*, 2729−2735. (c) Marraud, M.; Aubry, A. *Biopolymers* **1996**, *40*, 45−83. See also ref 29c.
(53) For a discussion of Cγ-puckering in Pro, see: Shoulders, M. D.; Kotch, F. W.; Choudhary, A.; Guzei, I. A.; Raines, R. T. *J. Am. Chem. Soc.* **2010**, *132*, 10857−10865.
(54) Shapovalov, M. V.; Dunbrack, R. L. *Proteins: Struct., Funct., Genet.* **2007**, *66*, 279−303.
(55) (a) Zhou, A. Q.; O'Hern, C. S.; Regan, L. *Biophys. J.* **2012**, *102*, 2345−2352. (b) Zhou, A. Q.; Caballero, D.; O'Hern, C. S.; Regan, L. *Biophys. J.* **2013**, *105*, 2403−2411. (c) Caballero, D.; Smith, W. W.; O'Hern, C. S.; Regan, L. *Proteins: Struct., Funct., Genet.* **2015**, *83*, 1488−1499. (d) Caballero, D.; Virrueta, A.; O'Hern, C. S.; Regan, L. *Protein Eng., Des. Sel.* **2016**, *29*, 367−376.
(56) For a review of H-bonding in the solid state, see: Steiner, T. *Angew. Chem., Int. Ed.* **2002**, *41*, 48−76.
(57) For a discussion of τ-angle distributions, see: (a) Malathy Sony, S. M.; Saraboji, K.; Sukumar, N.; Ponnuswamy, M. N. *Biophys. Chem.* **2006**, *120*, 24−31. See also ref 43. For a discussion of τ-angles in Pro-residues, see: (b) Karplus, P. A. *Protein Sci.* **1996**, *5*, 1406−1420.
(58) For a related example, see: Jakobsche, C. E.; Choudhary, A.; Miller, S. J.; Raines, R. T. *J. Am. Chem. Soc.* **2010**, *132*, 6651−6653.
(59) (a) Newberry, R. W.; Orke, S. J.; Raines, R. T. *Org. Lett.* **2016**, *18*, 3614−3617. (b) Siebler, C.; Maryasin, B.; Kuemin, M.; Erdmann, R. S.; Rigling, C.; Günenfelder, C. E.; Ochsenfeld, C.; Wennemers, H. *Chem. Sci.* **2015**, *6*, 6725−6730. See also ref 44.
(60) Bürgi, H. B.; Dunitz, J. D. *Acc. Chem. Res.* **1983**, *16*, 153−161.
(61) We acknowledge the caveats associated with drawing comparisons between X-ray crystal structures, NMR solution conformations, and enantioselectivity values that were obtained in different solvents. However, we do not anticipate this to be a source of significant deviation in the present context. Significant changes in peptide conformation have been observed upon switching from nonpolar to strongly H-bonding solvents. For example, see: Awasthi, S. K.; Shankaramma, S. C.; Raghothama, S.; Balaram, P. *Biopolymers* **2001**, *58*, 465−476. The solvents examined (EtOAc, PhMe, PhH, and THF) span a narrow dielectric range and are generally considered to be nonpolar solvents. Furthermore, in the rare cases in which we have observed solvent molecules in the crystallographic unit cells, they are not directly interacting with the peptides.
(62) This chart is not intended to be a frequency histogram, but rather it is meant to highlight the diversity we observed within this crystal structure library.
(63) For discussions of Acpc (and derivatives) in peptides, see: (a) Crisma, M.; Borggraeve, W. M.; Peggion, C.; Formaggio, F.; Royo, S.; Jiménez, A. I.; Cativiela, C.; Toniolo, C. *Chem.−Eur. J.* **2006**, *12*, 251−260. (b) Casanovas, J.; Jiménez, A. I.; Cativiela, C.; Pérez, J. J.; Alemán, C. *J. Phys. Chem. B* **2006**, *110*, 5762−5766. (c) Zanuy, D.; Ballano, G.; Jiménez, A. I.; Casanovas, J.; Haspel, N.; Cativiela, C.; Curcóm, D.; Nussinov, R.; Alemán, C. *J. Chem. Inf. Model.* **2009**, *49*, 1623−1629. (d) Fabiano, N.; Valle, G.; Crisma, M.; Toniolo, C.; Saviano, M.; Lombardi, A.; Isernia, C.; Pavone, V.; Di Blasio, B.; Pedone, C.; Benedetti, E. *Int. J. Pept. Protein Res.* **1993**, *42*, 459−465. (e) Benedetti, E.; Di Blasio, B.; Pavone, V.; Pedone, C.; Santini, A.; Barone, V.; Fraternali, F.; Lelj, F.; Bavoso, A.; Crisma, M.; Toniolo, C. *Int. J. Biol. Macromol.* **1989**, *11*, 353−360. (f) Valle, G.; Crisma, M.; Toniolo, C.; Holt, E. M.; Tamura, M.; Bland, J.; Stammer, C. H. *Int. J. Pept. Protein Res.* **1989**, *34*, 56−65. (g) Varughese, K. I.; Srinivasan, A. R.; Stammer, C. H. *Int. J. Pept. Protein Res.* **1985**, *26*, 242−251. See also refs 11c and 24a.
(64) Some type I/I′ β-turns similar to those we have observed were located in the CSD. This substructure was most often found in longer, helical sequences. For example, see: (a) Bunkóczi, G.; Schiell, M.; Vértesy, L.; Sheldrick, G. M. *J. Pept. Sci.* **2003**, *9*, 745−752. (b) Karle, I. L.; Flippen-Anderson, J.; Sukumar, M.; Balaram, P. *Proc. Natl. Acad. Sci. U. S. A.* **1987**, *84*, 5087−5091. (c) Karle, I. L.; Gurunath, R.; Prasad, S.; Kaul, R.; Rao, R. B.; Balaram, P. *J. Am. Chem. Soc.* **1995**, *117*, 9632. For some examples in shorter peptides, see: (d) Francis, A. K.; Iqbal, M.; Balaram, P.; Vijayan, M. *J. Chem. Soc., Perkin Trans. 2* **1982**, 1235−1239. (e) De Zotti, M.; Ballano, G.; Jost, M.; Salnikov, E. S.; Bechinger, B.; Oancea, S.; Crisma, M.; Toniolo, C.; Formaggio, F. *Chem. Biodiversity* **2014**, *11*, 1163−1191. (f) Ghasparian, A.; Moehle, K.; Linden, A.; Robinson, J. A. *Chem. Commun.* **2006**, 174−176. For some examples of type I′ hairpins that are not helical, see: (g) Karle, I. L.; Gopi, H. N.; Balaram, P. *Proc. Natl. Acad. Sci. U. S. A.* **2001**, *98*, 3716−3719. (h) Bandyopadhyay, A.; Misra, R.; Gopi, H. N. *Chem. Commun.* **2016**, *52*, 4938−4941.
(65) Gilli, P.; Pretto, L.; Bertolasi, V.; Gilli, G. *Acc. Chem. Res.* **2009**, *42*, 33−44.
(66) For example, see: (a) Denmark, S. E.; Burk, M. T. *Proc. Natl. Acad. Sci. U. S. A.* **2010**, *107*, 20655−20660. For a review on Lewis base catalysis, see: (b) Denmark, S. E.; Beutner, G. L. *Angew. Chem., Int. Ed.* **2008**, *47*, 1560−1638.
(67) For a review on *trans*/*cis* isomerization in peptides, see: (a) Fischer, G. *Chem. Soc. Rev.* **2000**, *29*, 119−127. For an example involving Pro, see: (b) Fischer, S.; Dunbrack, R. L., Jr.; Karplus, M. *J. Am. Chem. Soc.* **1994**, *116*, 11931−11937. (c) Wedemeyer, W. J.; Welker, E.; Scheraga, H. A. *Biochemistry* **2002**, *41*, 14637−14644.
(68) It is difficult to extract $^3J_{NH-H}\alpha$ values for the *i* and *i* + 3 residues of **3** + **1** and **3** + **2**, owing to the lower peak resolution due to the presumed catalyst−substrate complexation.
(69) (a) Koshland, D. E., Jr. *J. Cell. Comp. Physiol.* **1959**, *54*, 245−258. (b) Koshland, D. E., Jr.; Mémethy, G.; Filmer, D. *Biochemistry* **1966**, *5*, 365−385. For reviews, see: (c) Changeux, J.-P. *Annu. Rev. Biophys.* **2012**, *41*, 103−133. (d) Johnson, K. A. *J. Biol. Chem.* **2008**, *283*, 26297−26301. (e) Herschlag, D. *Bioorg. Chem.* **1988**, *16*, 62−96.
(70) For related examples, see: (a) Milo, A.; Bess, E. N.; Sigman, M. S. *Nature* **2014**, *507*, 210−214. (b) Gustafson, J. L.; Sigman, M. S.; Miller, S. J. *Org. Lett.* **2010**, *12*, 2794−2797. (c) Sigman, M. S.; Harper, K. C.; Milo, A. *Acc. Chem. Res.* **2016**, *49*, 1292−1301.

DOI: 10.1021/jacs.6b11348
J. Am. Chem. Soc. 2017, 139, 492−516